The effect of GMO nanoparticles on skin structure and penetration of a model compound by CARS and fluorescence microscopy

Effekten af GMO nanopartikler på hudens struktur og penetration af et modelstof ved CARS og fluorescens mikroskopi

Bachelor Report by Suzanna Cieslak Frank Frederiksen

Department of Physics, Chemistry and Pharmacy

University of Southern Denmark Odense

May 2016

Supervisor

Judith Kuntsche and Jonathan Brewer

Content

Abstract

The penetration enhancing effect of cubosome dispersions composed of glycerol monooleate (GMO) both with and without diclofenac sodium was investigated on human skin. Cubosome dispersions were prepared by dual centrifugation and particle sizes were measured by DLS, light microscopy, AF4 and LD-PIDS. The particle diameters varied depending on which method was used for size analysis. Furthermore, the formulations were spiked with deuterated GMO for easier characterization of the penetration of the formulations by CARS microscopy. However, due to a low signal from the CD bonds or background noise, no clear signal was detected. Though, the skin structure was investigated by CARS and visualized. To investigate the penetration enhancing effect of the prepared formulations by fluorescence microscopy the formulations, both with and without diclofenac sodium, were added the fluorophore DiI. The stained formulations were allowed to penetrate into the skin for 24 hours in Franz diffusion cells. The penetration of a control solution only containing DiI was also investigated for comparison. The skin samples containing the stained formulations were studied using LSCM. The results indicate, that the diclofenac-loaded particles penetrated the epidermis of the skin to a high extent because of the high intensity observed. The formulations without diclofenac still penetrated the epidermis but to a lesser extent. The DiI control solution barely penetrated the skin and most DiI gathered in the stratum corneum.

Dansk resumé

Penetrationen af kubosomer bestående af glycerol monooleat (GMO) både med og uden diclofenac natrium er undersøgt på huden. Dispersionerne er forberedt vha. centrifugering, og partikelstørrelser er blevet bestemt vha. DLS, lysmikroskopi, AF4 og LD-PIDS. Resultaterne viste, at diametrene varierede afhængigt af hvilken metode, der var benyttet til undersøgelsen. Yderligere blev deuteret GMO tilføjet formuleringerne for nemmere karakterisering af formuleringernes penetration på huden i CARS mikroskopet. På grund af lave signaler fra CD bindingerne eller støj i baggrunden blev intet klart signal opfanget. Dog blev huden undersøgt vha. CARS og visualiseret. For at undersøge penetrationen af de forberedte formuleringer på huden vha. fluorescensmikroskopi blev formuleringerne indeholdende diclofenac natrium og uden diclofenac natrium tilsat fluoroforen DiI. De farvede formuleringer penetrerede herefter huden i 24 timer i Franz diffusionskamre. Derudover blev penetrationen af en kontrolopløsning kun indeholdende DiI undersøgt til sammenligning. Hudprøverne indeholdende de farvede formuleringer blev undersøgt i LSCM. Resultaterne af dette viste, at de diclofenac-indeholdende partikler penetrerede epidermis i huden i høj grad, hvilket observeres af den høje intensitet. Formuleringerne uden diclofenac natrium penetrerede stadig epidermis men i mindre grad. DiI kontrolopløsningen penetrerede knap nok huden, og det meste DiI samledes i stratum corneum.

Abbreviation list

AF4	Asymmetrical flow field-flow fractionation
CARS	Coherent anti-Stokes Raman scattering
dGMO	Deuterated glycerol monooleate
DiI	Dioctadecyl-tetramethylindocarbocyanine perchlorate
DLS	Dynamic light scattering
GMO	Glycerol monooleate
LSCM	Laser scanning confocal microscopy
LD	Laser diffraction
MALLS	Multi-angle laser light scattering
PDI	Polydispersity index
PIDS	Polarized intensity differential scattering
SC	Stratum corneum

1. Introduction

1.1. Aims of the project

The objective of this project was to investigate the penetration enhancing effect of cubosomes on skin. Cubosome dispersions were prepared by dual centrifugation and characterized by dynamic light scattering (DLS), light microscopy, asymmetrical flow field-flow fractionation (AF4) and laser diffraction polarized intensity differential scattering (LD-PIDS). Coherent anti-Stokes Raman scattering (CARS) microscopy and laser scanning confocal microscopy (LSCM) was used to investigate skin structure and the effect of the cubosomes on the penetration of a hydrophobic model dye.

1.2. The skin barrier

The skin is the largest organ of the body and due to its ease of drug administration, it represents an interesting route for drug delivery [1, 2]. The major function of the skin is to protect the body against UV radiation, free radicals, physical, chemical, immunogenic factors as well as pathogens. The skin also functions in thermoregulation, perform as a sensory organ, and has endocrine functions e.g. vitamin D synthesis [3]. Moreover, it excretes urea, salts and water which are lost through sweat.

The skin consists of two distinct layers: The outermost layer, the epidermis, and the layer beneath, the dermis (Figure 1). Just beneath the dermis, the subcutis is found which is a fatty layer and it is not a part of the skin but shares some of the skin's functions such as preventing heat loss from the body. The dermis consists of connective tissue containing collagen and elastic fibers. Furthermore, the dermis contains capillaries which provide the epidermis with nutrients. The outermost layer, the epidermis, can further be divided into five layers [4, 5]. The inner layer of the epidermis (closest to the dermis) is called stratum basale and consists of mostly stem cells. From here the cells differentiate and form the upper epidermal layers with the stratum corneum (SC) being the uppermost layer. The SC consists of 20-30 layers of dead cells (called corneocytes) which are characterized by flat membraneous sacs filled with keratin [4]. Between these cells there is a lipid layer which is mainly composed of ceramides [4]. The SC is organized in a brick-and-mortar arrangement [6]. This arrangement of the protein-enriched corneocytes ("bricks") contribute to the tortuosity of the transport of water or other molecules which traverse the SC and the hydrophobic lipid layer ("mortar") provides a water-tight barrier [3]. These characteristics help to protect the skin against abrasion and penetration and it makes it a tortuous pathway for compounds such as drugs to traverse the SC and hence the skin [3, 4].

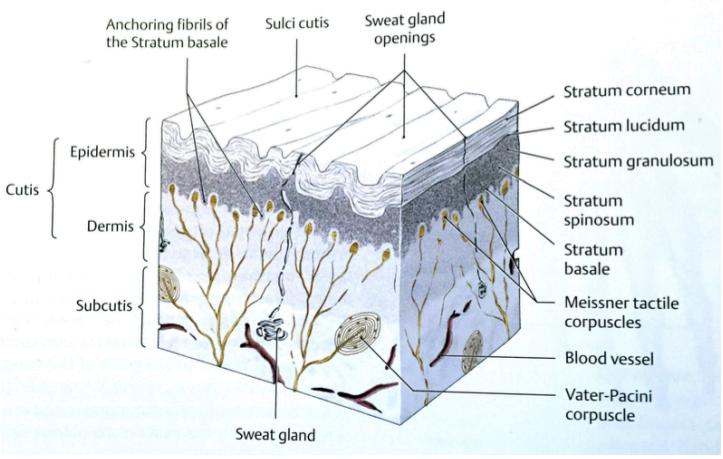

Figure 1: The structure of the skin. The epidermis consists of five layers where the outermost layer is stratum corneum. Just beneath the epidermis, dermis and subcutis are found [5].

1.3. Cubosomes and transdermal drug delivery

For drug delivery, the drug can be delivered either through transdermal delivery or dermal delivery depending on the site of action. In transdermal delivery the drug diffuses through the different layers and into the systemic circulation and in dermal delivery the drug targets sites within the skin [7].

It is a challenge to produce pharmaceuticals for dermal and especially transdermal delivery due to the structure of stratum corneum. Therefore, various strategies to overcome the barrier of the skin have been developed. A common method for this purpose is to use chemical penetration enhancers (e.g. ethanol) but other methods for dermal and transdermal delivery have also been developed such as microneedles, ultrasound and colloidal drug carriers [1]. Colloidal drug carriers include microemulsions, micelles, liposomes and lipid nanoparticles (e.g. nanostructured lipid carriers or cubic nanoparticles). Cubic nanoparticles (or cubosomes) are based on a cubic lyotropic liquid crystalline phase. Besides lyotropic liquid crystals which are formed by amphiphilic substances in the presence of a suitable solvent, liquid crystals can also be formed by their temperature dependence (thermotropic liquid crystals [8]). The cubic liquid crystalline phase is transparent and isotropic and may be physically stable in excess of water [9]. When the cubic liquid crystalline phase is stable in the presence of water, cubosomes can be produced. Surface active agents such as poloxamers and phospholipids can stabilize the cubic phase and a colloidal dispersion is made [10].

When adding water to a surfactant, different phases occurs depending on the concentration of the surfactant [8]. First, the transition from the spherical micellar structure to a more rod-like micelle occurs. By further increasing the concentration of surfactant in the liquid crystalline phase, first a hexagonal phase will occur and then a lamellar phase. In some surfactant systems the cubic phase will occur between these two phases. The most common cubic phase is a micellar cubic phase where spherical micelles are closely packed. With use of certain lipids and with a high water content (~20-40% at room temperature) a more complex cubic phase (bicontinous cubic phase) is formed [8, 11]. A common example of a lipid forming a bicontinous cubic phase is the amphiphilic polar lipid glycerol monooleate (GMO, Figure 2) [12]. These cubic nanoparticles consist of hydrated glycerol monooleate bilayers extending in three dimensions separating two identical water channel systems [13]. Both the polar lipid and the bilayered particle structure can be an advantage in drug penetration and/or permeation [9, 14]. Moreover, GMO has skin-penetrating effects itself [14].

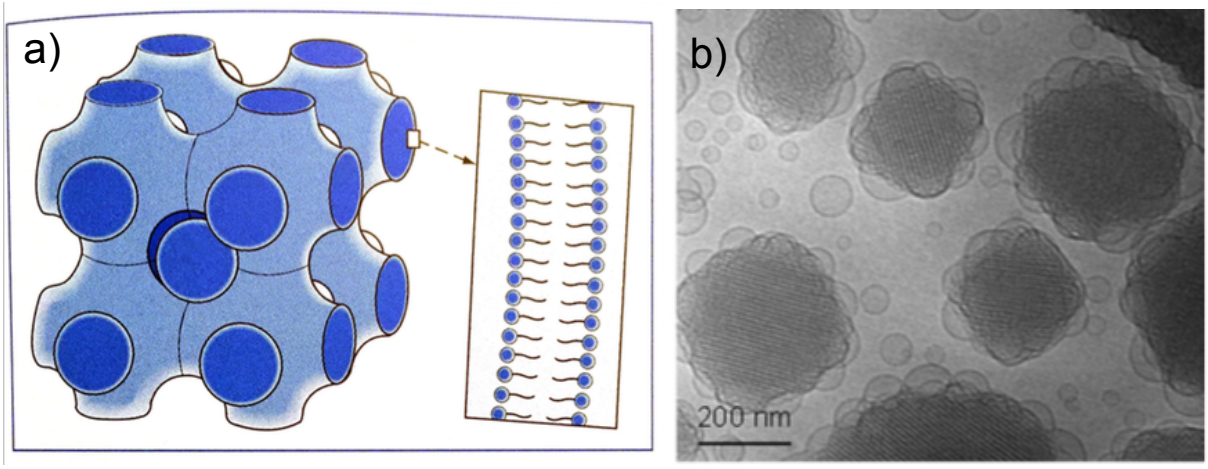

Figure 2: Cubosomes. a) Structure of the bicontinous cubic phase of GMO. The enlargement shows the lipid bilayer [8]. b) Cryo-electron microscopic image of cubic nanoparticles [10].

To stabilize GMO nanoparticles or cubosomes, another surfactant is usually added, such as poloxamer 407 [11, 12]. Usually P407 is applied at a concentration of 12% (in proportion to the total amount of lipid and stabilizer in the formulation) [11].

Besides GMO and poloxamer, the formulations prepared in this project contain the active ingredient diclofenac sodium. Diclofenac is used against inflammation and it also contains analgesic and antipyretic properties [15]. There are different dermal drug formulations containing diclofenac on the market e.g. Solaraze gel [16] and Voltaren gel [15]. The site of action of the active ingredient, diclofenac, depends on target site and is determined by the excipients in the formulation. In this study cubosomes loaded with diclofenac were investigated and some formulations were prepared with deuterated GMO for CARS microscopy (see below).

To prepare dispersions of cubic nanoparticles, different methods can be used. The two main methods in the production of cubosomes are the ‘bottom-up’ and ‘top-down’ approaches [12]. In the bottom-up approach cubosomes are formed at room temperature with a minimal energy input. In the top-down approach high energy is applied such as high-pressure homogenization or sonication. Dual centrifugation is an example of a top-down approach (Figure 3). It is a centrifugation method where the vial (containing the formulation) is turned around the main rotation axis by a defined speed and acceleration. Simultaneously, the vial itself is turned around its own center (in the same direction as the main rotation). This results in the sample being pushed both outwards by the main rotation and inwards due to the rotation of the vial around its own center. The main rotation arm of the dual centrifuge forms an angle of about 40° with the rotation plane which results in the sample being forced into the corner between the bottom and the wall of the vial. Furthermore, there are other ways to make the formulation even more homogenous. By adding glass beads to the formulation in the vial in the dual centrifuge the sample will be more homogenous than without glass beads [17].

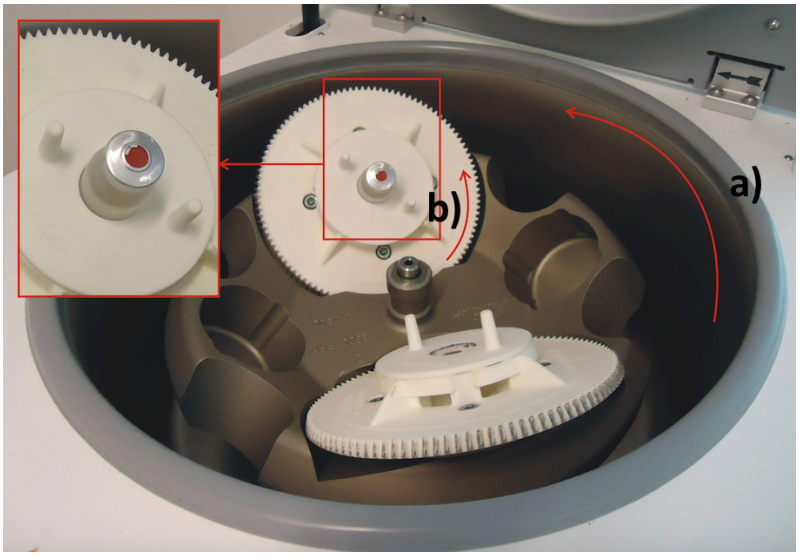

Figure 3: The dual centrifuge. The vial is turned around a) the main rotation axis and the vial itself is at the same time turned around b) its own center.

1.4. Particle size determinations

Particle size and particle size distribution are important quality parameters for pharmaceutical dispersions (e.g. emulsions and suspensions). There are several methods for size determination and three different methods have been applied in the present project.

Dynamic light scattering (DLS) is a well-established method for size determination of particles in the sub-micron size region [18]. The hydrodynamic diameter is a value that tells about how fast a particle diffuses within a fluid. It is a value of a sphere having the same diffusion coefficient as the particle. The hydrodynamic diameter is measured from the particle's Brownian motion which is the random movement of particles caused by collisions with the other molecules in the sample. DLS measures the fluctuations in the light scattering patterns caused by particles undergoing Brownian motion. The rate of intensity fluctuations of scattered light depends on the velocity of diffusion e.g. a higher diffusion velocity will result in more rapid intensity fluctuations.

The typical DLS instrument is composed of a laser, which provides monochromatic light focusing on the sample in a cell. A detector placed at an angle of 90° to the cell measures the scattered light. However, modern instruments such as the Delsa Max detect the scattering light at an large angle (backscattering) to minimize multiple scattering and thus enabling size determinations of samples with higher concentrations. Between the laser and the cell an attenuator is usually placed. The attenuator is used to regulate laser intensity to avoid too high intensity of scattered light at the detector. If too little light is scattered from the sample (e.g. low concentration or very small size) the amount of scattered light must be increased and the attenuator is used to increase the laser power. If too much light is scattered from the sample (e.g. high concentration or large particle size) the attenuator is used to decrease the intensity of the laser. The detector signals are passed to a digital correlator which converts the intensity of the scattered light into an auto-correlation function, which is then used to calculate the mean particle size (z-average) together with the polydispersity index (PDI, a measure for the relative width of the particle size distribution), which gives information about sample homogeneity (e.g. how well the mean particle size is described by this single mean value; cumulant analysis, [18, 19]). DLS is limited by the size range and should therefore be combined with other methods (e.g. light microscopy) to check for the presence of large particles in the µm-size range, which

cannot be detected by DLS. Another limitation is determining the size distribution and therefore it can be combined with AF4/MALLS.

Due to the combination of sample fractionation and size determination, accurate information about size distributions can be obtained by asymmetrical flow field-flow fractionation (AF4) coupled with multi-angle laser light scattering (MALLS). AF4 is able to separate colloidal components over a wide size range (about 5 kDa and 1 µm in standard setup used in this study) and many variabilities in conditions are possible which allows the separation of specific samples [20]. In Figure 4, the different components of the AF4 instrument used in this study are shown. The instrument consists of an isocratic HPLC pump system (degasser, pump and autosampler) which is connected to Eclipse (AF4) and detectors. The most important parts in this setup is the separation channel and the AF4 which controls the conditions of the flow within the channel and the MALLS detector, which measures light scattering and provides accurate information of the particle sizes.

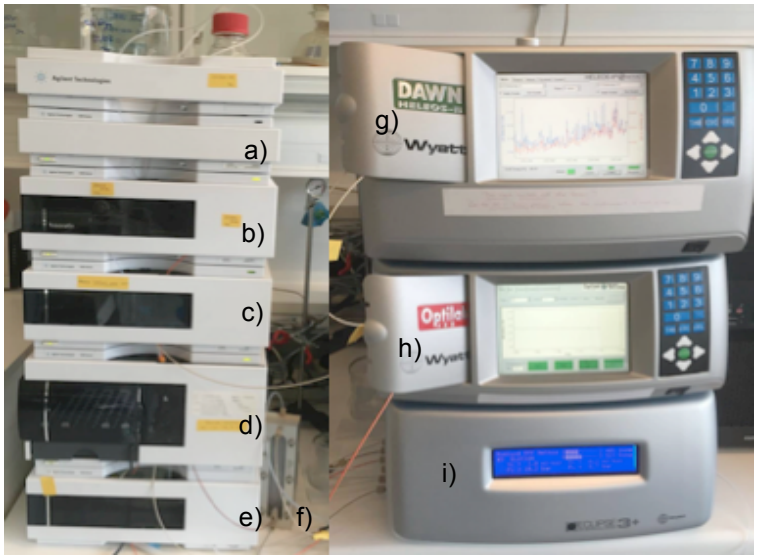

Figure 4: AF4/MALLS setup: a) Degasser b) Isocratic pump c) Variable wavelength detector d) Autosampler e) Thermostat f) Separation channel g) MALLS detector h) dRI detector and i) Eclipse (AF4).

By AF4, the particles are separated depending on their hydrodynamic size, which can be calculated by their elution time [20]. However, this approach requires accurate knowledge about the channel height (normally not known, as the membrane swells in contact with the carrier liquid) and may be complicated when different cross flow gradients are applied. By coupling the separation system with MALLS a direct size determination is achieved. The separation happens in the channel where two plates are separated by a spacer (Figure 5). The upper plate is impermeable whereas the bottom plate is permeable for the carrier liquid and covered by an ultrafiltration membrane (also called accumulation wall). The flow conditions in the channel are determined by a laminar flow through the channel (detector or channel flow) and by applying a cross flow (force field) perpendicularly to the membrane. This cross flow will “push” the molecules or particles towards the membrane and this causes the sample fractionation.

The separation process generally requires three steps. In the first two steps, injection and focusing, the carrier liquid enters the channel from both inlet and outlet. The flow will be balanced to meet just under the injection port. When the whole sample has been injected, the sample will be focused in a thin band and is forced toward the membrane on the bottom plate due to the focus flow (leaving the channel over the membrane). Afterwards, in the third step, the

flow is turned to elution mode. Here the carrier liquid will only enter the channel from one inflow port (“Inflow” and exit from the outflow port further to the detectors). A parabolic flow profile is generated in the channel due to the laminar flow of the liquid. At a given cross flow, the larger particles will be pushed more to the bottom of the channel as the smaller particles having a higher diffusion rate thus reaching an equilibrium position higher in the channel. This causes the small particles to move faster within the channel than larger particles and the small particles will be eluted first [21].

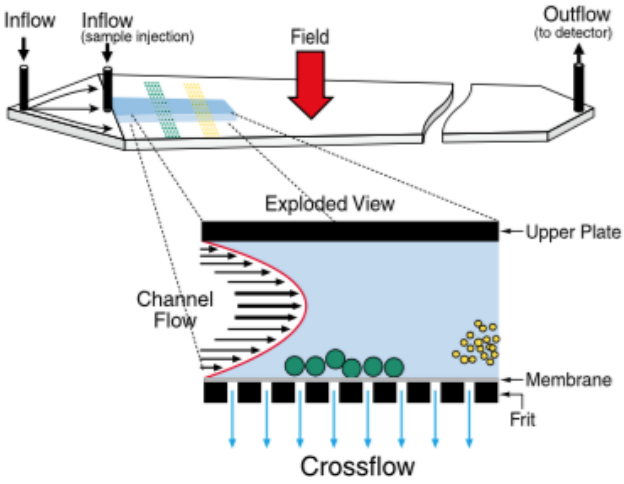

Figure 5: The principle of AF4 separation. A parabolic flow profile is obtained in the separation channel and due to the cross flow applied the larger particles will be pushed down to the bottom of the channel. The small particles with a higher diffusion rate will reach an equilibrium position higher in the channel and be eluted faster than the larger particles [21].

Another method for obtaining information about size distribution is from laser diffraction (LD) in combination with polarized intensity differential scattering (PIDS). LD-PIDS measures the scattering of light by the particles in the sample over a broad size range (about 40 nm up to a few mm). This can be described by the Mie theory which explains the interaction of light with a particle of random size as a function of angle and given that factors as wavelength and polarization of the light are known. Furthermore, the particle has to be smooth, spherical, homogenous and have a known refractive index [22]. At small angles the light scattering from the spheres produce patterns which are centrally symmetric. Large particles will produce intensities of scattering which are concentrated at small angles mostly due to the effects of diffraction from the edge of the particle. When particles become smaller it is more difficult to determine their size values by diffraction, because of the reduction of the scattering intensity pattern. By applying PIDS to the measurement method the polarization effects of light scattering at high angles can be obtained and the size limit can be lowered to 40 nm. The PIDS signal is measuring the difference in scattering intensity between the polarized light beam in the vertical and horizontal direction. The scattering intensity is obtained from the motion of electrons in the sample and there will be an oscillation of the light. If the detector is facing the direction of this oscillation no scattering will be received [22].

1.5. Methods on investigating the formulations on skin

Skin penetration and permeation can be investigated in different ways e.g. by using diffusion cells which are typically used for in vitro studies of transdermal delivery [23] but can also be used to study dermal delivery. Different types of diffusion cells can be chosen depending on the

desired flow in the system [24]. A type of diffusion cell is the Franz cells which is a typical static flow cell where the receptor fluid is stirred (Figure 6).

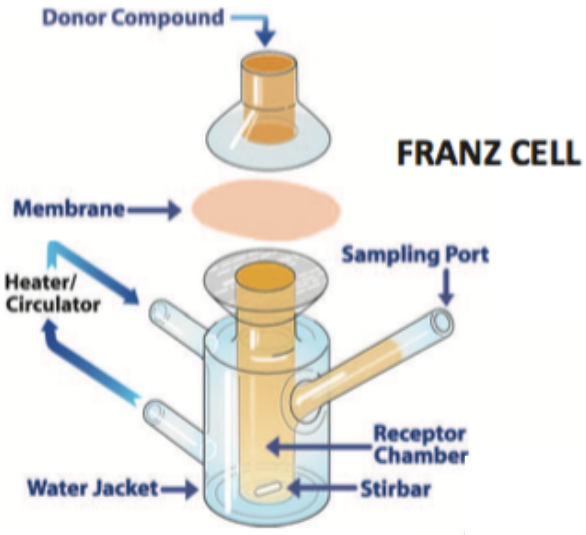

Figure 6: Franz cell. The arrangement consists of a receptor chamber and a donor compound where a membrane is clamped in between [24].

The experimental setup should mimic the in vivo situation and therefore, the receptor fluid chosen should simulate the physiological conditions. Between the receptor chamber and the donor compartment a membrane is clamped and formulation can thereafter be applied. The membrane can be e.g. polymeric membranes or human skin (or epidermis) [24]. The amount of permeated drug can be determined by withdrawing samples from the receptor phase. To get information about drug penetration (e.g. drug amount within the skin) tape stripping (removal of SC) [9] and cryo-sectioning of the dermis are methods which can be used.

Drug penetration can also be investigated and visualized by microscopic methods. This can be done by e.g. conventional fluorescence microscopy, two-photon excited fluorescence microscopy (TPEF) [25] or laser scanning confocal microscopy (LSCM) [26, 27]. A drawback of these techniques is that a fluorophore is needed. Coherent Raman scattering (CRS) microscopy is a label-free imaging technique which allows a three-dimensional mapping of molecules. CRS microscopy can be accomplished by either detecting stimulated Raman scattering (SRS) or coherent anti-Stokes Raman scattering (CARS) [28]. CARS microscopy is based on the characteristic vibrational contrast of the bonds in the molecules investigated [29] which is explained later. The CARS microscope which has been used in this project is shown in Figure 7. The important components in a CARS microscope is a light microscope with four detectors attached (epi-CARS (E-CARS), forward-CARS (F-CARS), epi-second harmonic generation (E-SHG) and forward-second harmonic generation (F-SHG)) and a pump and a Stokes laser. The components are connected to a computer where the image is viewed.

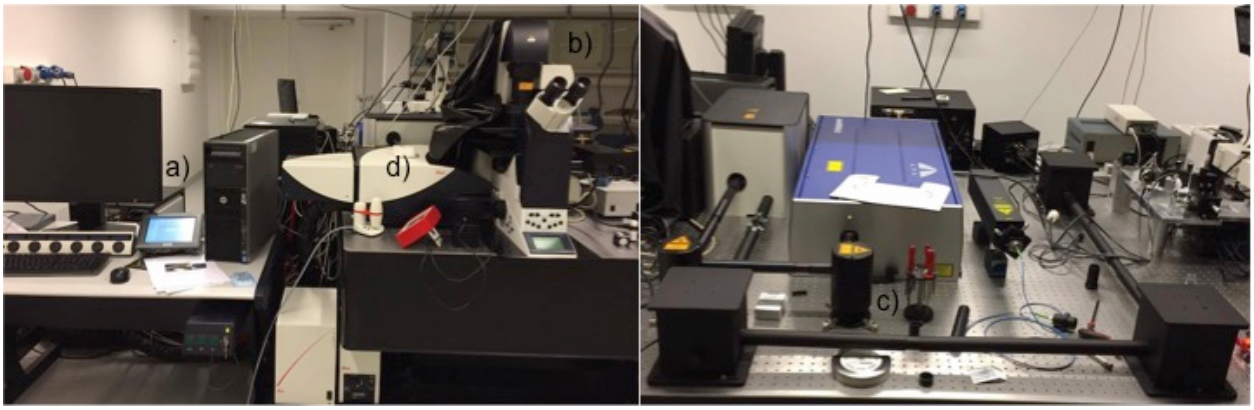

Figure 7: CARS and fluorescence microscopy. a) Computer used for imaging. b) Light microscopy with attached detectors. c) Stokes and pump laser. d) Scan head for fluorescence microscopy.

A schematic presentation of the CARS setup can be seen in Figure 8. A laser (Nd:VYO_4) pumps the optical parametric oscillator (OPO) with a dual wavelength. From the OPO, the pump and Stokes lasers are scanned over the sample by use of a scanner (XY scanner). The CARS signal is generated in both the forward and backwards direction. The signal in the forward direction goes through a condenser and a filter where the excitation beams are separated until it reaches the F-CARS detector [30]. The other signal goes through a filter and reaches the E-CARS detector or it will be detected by a descanned detector.

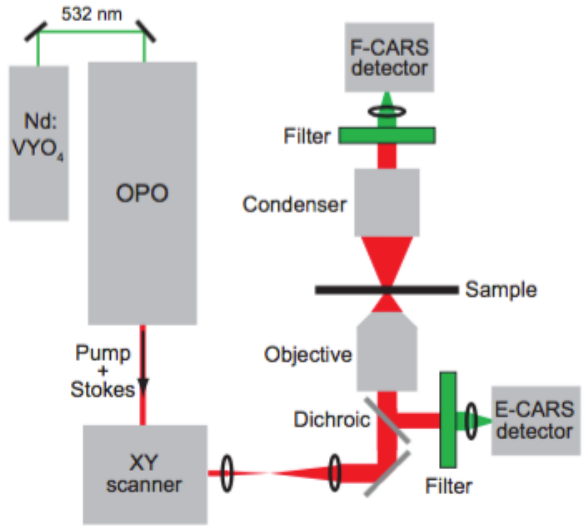

Figure 8: Schematic presentation of collinear beam-scanning in the CARS microscope [30].

The frequency of the pump laser can be given by ω_p and the frequency of the Stokes laser can be given by ω_s. The difference between the frequencies, $\Delta\omega = \omega_p - \omega_s$, creates the vibrational contrast in CARS when the difference between the pump and Stokes lasers ($\Delta\omega$) are equal to the frequency of the vibration in the specific bond in the molecule to be imaged. This characteristic vibrational state is used to produce sufficient signal above noise from the surroundings for visualization (Figure 9, virtual state 1). First, the pump laser excite the molecules from the ground state to a virtual state. Simultaneously, the Stokes laser radiates the molecule at a longer wavelength forcing the molecule from the virtual state to the desired vibrational energy state which is adjusted to the specific vibrational energy of the relevant molecule due to the tunable pump beam. The pump laser will then excite the molecule to another virtual state (Figure 9, virtual state 2). From this state the molecules will relax back to

the ground state releasing the CARS photons which are detected by a photomultiplier detector. These photons are used for the visualization of the sample [29].

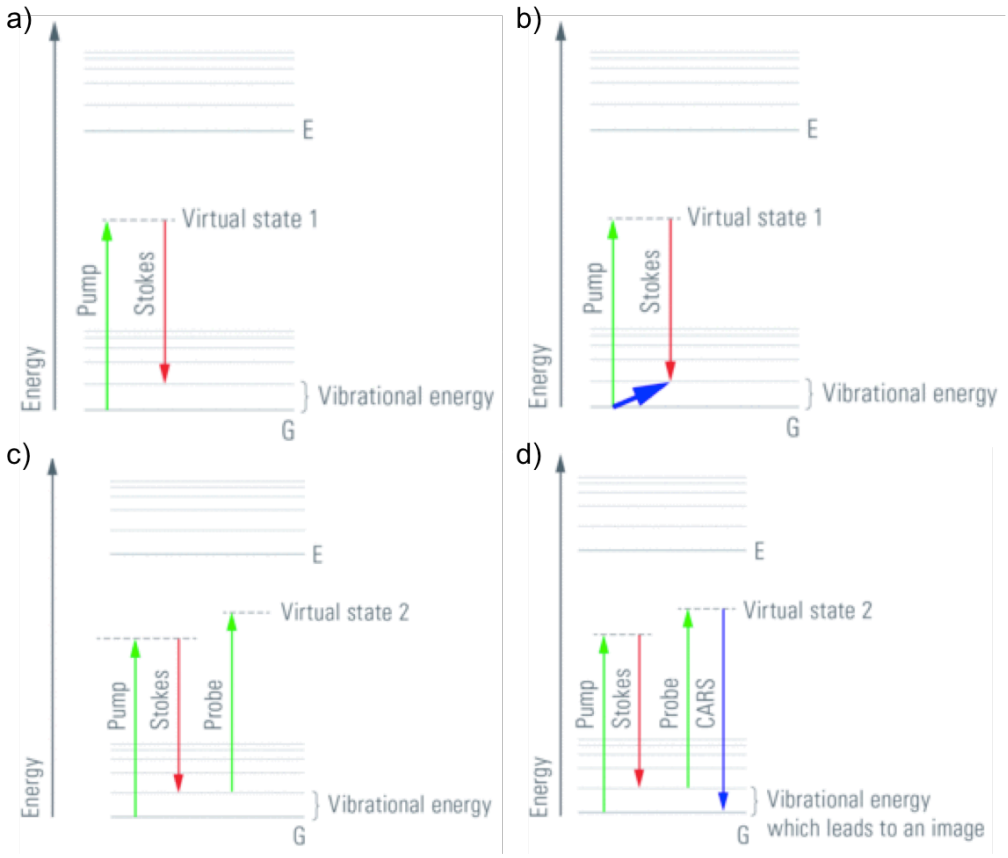

Figure 9: The CARS process of visualization. a) Excitation of the molecule by the pump laser to the virtual state. b) The Stokes laser will force the molecule to the desired vibrational energy. c) The molecule will be elevated to a new virtual state. d) The molecule will relax from the virtual state and the photons released are used for imaging [29].

In many studies, a specific small molecule e.g. inside a cell is needed to be imaged. This can be done by substituting hydrogen from e.g. a CH bond with deuterium which is similar to isotope tracking and shown to be an effectual method [31]. The deuterium in a CD bond is heavier than hydrogen and this vibrational energy will therefore be possible to specifically detect in a Raman spectra. A Raman spectra shows the intensity as a function of wavenumber. The stronger the intensity at a given wavenumber, the stronger the signal. In this project deuterated GMO has been used for detection in the prepared formulations. By using deuterium, it should be possible to distinguish the CH bonds deriving from the skin lipids from the CD bonds in the lipid chains in GMO due to the different energy and wavelength. A strong signal from the CD bond in the deuterated GMO will be seen at 2100 cm^{-1} in a Raman spectra which is otherwise a “silent” region [30]. The specific molecule can therefore be imaged by tuning into the specific CD frequency at 2100 cm^{-1}.

For fluorescence microscopy, a dye with fluorescent properties (fluorophore) is needed to label the formulations [10]. The highly lipophilic DiI can be used as a fluorescent label to trace lipid nanoparticles in cells without a covalent link [32]. Furthermore, it is worth noticing that DiI is very stably incorporated into lipid nanoparticles and liposomes, e.g. release and transfer to other lipophilic phases only occurs very slowly [33]. A fluorophore has an emission and an absorption spectrum [26]. The excitation laser must be matched with the absorption spectrum, while the

detection must be matched to the emission spectrum [27] which for DiI is found in the region of the visible spectrum with an emission maximum of 565 nm (Figure 10) [34].

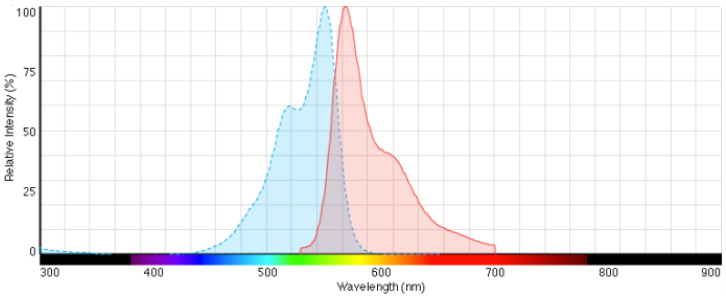

Figure 10: Fluorescence spectra for DiI. The x-axis illustrates the colors seen in the visible spectrum. The y-axis is the relative intensity (%). Blue dotted line: Absorption spectrum. Red full line: Emission spectrum [35].

In this study a laser scanning confocal microscope (LSCM) is used to visualize the fluorescent particles. The confocal microscope coupled to the CARS microscope is seen in Figure 7. In LSCM, the fluorescence emitted occurs throughout the entire depth of the sample [36] and the lights path can be described by a ray path (Figure 11). Here, an objective is used to focus the laser beam onto the sample. The laser beam is guided across the sample (via the dichroic mirror) and the sample will be irradiated point by point. The fluorescence radiated from each point will be collected by the objective and directed to a detector through a dichroic beamsplitter. The wavelength range which is investigated (e.g. the region of emission of DiI) is selected through the emission filter. When compared to a conventional microscope the important part of the LSCM is the pinhole which is found in front of the detector on a plane conjugate to the focal plane. Light which comes from other planes than the focal plane will be out of focus when it strikes the pinhole and will be rejected. Therefore, the light which passes the pinhole comes from the in focus plane [27]. Thus the pinhole enables optical sectioning in thick samples by preventing detection of out-of-focus light [27, 36].

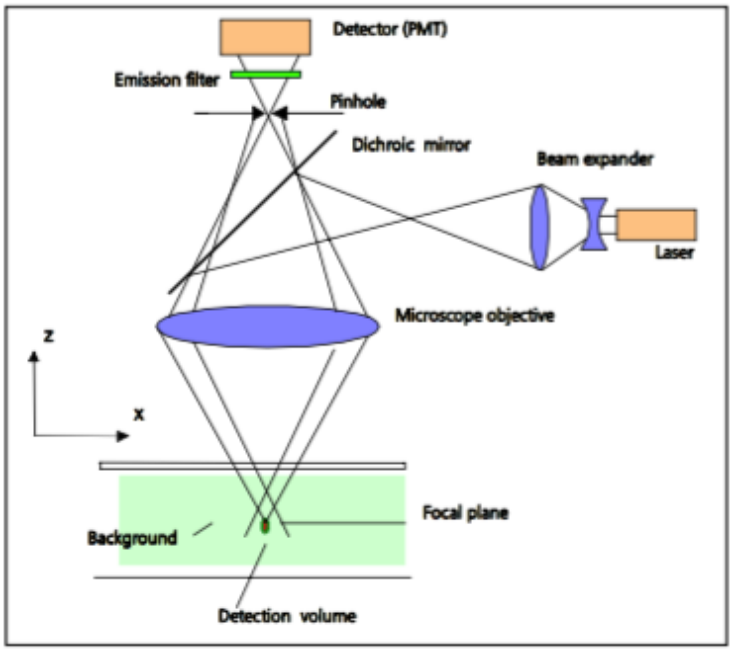

Figure 11: Diagram showing the function of the pinhole in LSCM [27]. The ray diagram shows how out-of-focus light is rejected by the pinhole, while the focused light passes through.

2. Material and methods

2.1. Materials

Specifications and information about chemicals used in this project are summarized in Table 1.

Table 1: Information and specifications about chemicals used in this project.

	Chemical	**Batch number***	**Supplier***
TRIS buffer (1.0 L)	TRIZMA pre-set crystals pH 7.4	056H5723	Sigma-Aldrich
	Glycerol, anhydrous	BCBH7875V	Sigma-Aldrich
	Sodium azide	BCBM5389V	Sigma-Aldrich
	Milli-Q water	n.a.	Millipore
GMO-formulations	Glycerol monooleate	4010989490	Rylo Mg 19 Pharma
	Poloxamer 407	WPCE634B	BASF
	Diclofenac sodium	BCBN3367V	Sigma-Aldrich
	Glass beads (2 mm)	n.a.	n.a.
	(±)-Glyceryl-1,1,2,3,3-d_5 1-Monooleate (dGMO), 98.3% D	X-488	CDN Isotopes
DiI stock solution	Dioctadecyl-tetramethylindocarbocyanine perchlorate (DiI)	BCBJ6016V	Sigma-Aldrich
	Ethanol, 99.5%	15K040502	VWR Chemicals

* Abbreviation for batch number and supplier: n.a. = not available

2.2. Preparation of TRIS buffer

10 mM TRIS buffer pH 7.4 containing 2.25% (w/v) glycerol for isotonization and 0.02% (w/v) sodium azide for preservation was prepared at a batch size of 1.0 L. First, TRIZMA pre-set crystals pH 7.4, sodium azide and glycerol were weighed in separate beakers (Table 2, for calculations see Appendix I). A suitable amount of Milli-Q water was added to the solid compounds and to glycerol to facilitate quantitative transfer into a 1.0 L volumetric flask. All beakers were rinsed with Milli-Q water at least three times to be sure that all the weighed compounds were completely transferred. Milli-Q water was then filled to around 80% of the final volume and the solution was mixed. The pH meter was calibrated with standard solutions pH 4.0 and pH 7.0 (Ion Analysis, Metrohm), and the pH of the solution was measured (pH 7.3). The volumetric flask was then filled to the final volume (1.0 L), mixed and then filtered by vacuum filtering (500 mL, Nalgene®, membrane pore size of 0.1 µm, PALL).

Table 2: Calculated and weighted masses for 1 L TRIS buffer.

Chemical	**Calculated mass**	**Weighted mass**
TRIZMA pre-set crystals	1.516 g	1.5178 g
2,25% glycerol	22.500 g	22.4966 g
0,02% sodium azide	0.200 g	0.1993 g
Milli-Q water	ad. 1.0 L	ad. 1.0 L

2.3. Preparation of GMO-formulations by dual centrifugation (DC)

Eight formulations both with and without diclofenac sodium were prepared in total (four of each, Table 3, for calculations see Appendix I). One formulation with diclofenac sodium and one without diclofenac sodium were prepared by adding deuterated GMO (dGMO). Both GMO and dGMO were stored in a freezer and allowed to warm up to room temperature before handling. GMO (and if applicable dGMO), poloxamer 407, TRIS buffer and glass beads were weighted into a 15 mL plastic vial for dual centrifugation (Table 3). The vials were sealed and then homogenized in the dual centrifuge (Zentrimix 380R dual centrifugation, Hettich Zentrifugen) at room temperature (25°C) at 2500 rpm. The diclofenac-containing formulations were centrifuged twice for 15 minutes (30 minutes in total) and the drug-free formulations twice for 30 minutes (60 minutes in total). The diclofenac-containing formulations had a gel-like structure and the drug-free formulations were liquid dispersions. After each centrifugation step a sample of 100 mg was withdrawn, transferred into an Eppendorf tube and dispersed in 100 mg TRIS buffer to obtain a 1:2 dilution. The sample in the Eppendorf tube was vortexed and stored at room temperature under light protection.

Table 3: The theoretical composition of the GMO-formulations and naming of the samples and the quantitative composition.

Naming	**Comments***	**dGMO (g)**	**GMO (g)**	**Poloxamer 407 (g)**	**Diclofe-nac so-dium (g)**	**TRIS buffer (g)**	**Glass beads 2 mm (g)**
Theoretical amounts		*0.050*	*0.880*	*0.120*	*0.150 or 0.050*	*ad 5.0*	*5.000*
GMO_D0_2	0% D, b.n. 2, DC for both 15 min and 30 min	0	0.8880	0.1218	0	3.9890	5.0049
GMO_D0_4	0% D, b.n. 4, DC for both 30 min and 60 min	0	0.8871	0.1267	0	4.0057	5.0057
GMO_D0_6	0% D, b.n. 6, DC for both 30 min and 60 min	0	0.8893	0.1211	0	3.9782	5.0269
dGMO_D0_8	Deuterated GMO, 0% D, b.n. 8, DC for both 30 min and 60 min	0.0518	0.8314	0.1210	0	3.9994	5.0219
GMO_D3_1	3% D, b.n. 1, DC for both 15 min and 30 min	0	0.8802	0.1251	0.1532	3.8514	5.0057
GMO_D1_3	1% D, b.n. 3, DC for both 15 minutes and 30 minutes	0	0.8830	0.1207	0.0505	3.9494	5.0091
GMO_D1_5	1% D, b.n. 5, DC for both 15 min and 30 min	0	0.8844	0.1207	0.0509	3.9554	5.0190
dGMO_D3_7	Deuterated GMO, 3% D, b.n. 7, DC for both 15 min and 30 min	0.0511	0.8343	0.1209	0.1500	3.8454	5.0188

* Abbreviations for comments: D = diclofenac sodium, b.n. = batch number, DC = dual centrifugation

2.4. Staining of GMO-formulations with DiI

A stock solution of 2 mg/mL DiI was prepared in 99.5% ethanol. 100 µL of the stock solution was added to 1.00 g of original formulation (non-diluted, dGMO_D3_7 and dGMO_D0_8). The samples were allowed to equilibrate for at least six days prior to use. A DiI control solution was made by adding 100 µL DiI stock solution to 1.00 g of 99.5% ethanol. This sample was made prior to use.

2.5. Light microscopy

All samples were viewed in a light microscope (Gundlach) equipped with a camera (PupilCam, Ken-A-Vision) to check for the presence of particles in the µm-size range. A drop from each diluted sample was placed on an object glass and covered with a cover slide. Samples were then viewed with an 10x and 20x objective. Three representative pictures of each formulation without diclofenac sodium were taken at both magnifications by use of Applied Vision software version 4.

2.6. Dynamic light scattering

The hydrodynamic diameter of the particles was measured by dynamic light scattering [18] using a DelsaMax Pro instrument (Beckmann Coulter). The temperature was set to 25.00°C and each sample was measured 6 times for 10 seconds. For the dispersant, a viscosity of 2% glycerol was used. Before starting the analysis, it was checked that the correlation function at the display on the DLS instrument was stable. Measurements were done in plastic cuvettes filled with TRIS buffer (about 500 µL) and 5 µL sample or 10 µL sample were added and mixed with the buffer. Particle size measurements were carried out after defined periods of time (3, 10, 36 and 56 days after preparation). In total two measurements (sample preparations with both 5 µL and 10 µL sample added to the cuvette) were done for each formulation at each time point (unless otherwise stated). Results are given as the hydrodynamic diameter (z-average) and the polydispersity index (PDI) calculated by the instrument (cumulant analysis, DelsaMax software version 1.0.1.6). Results of all measurements are summarized in Appendix II.

2.7. AF4/MALLS

Particle size and size distribution were also determined by AF4/MALLS. The samples were fractionized by an Eclipse 3+ AF4 separation system (Wyatt) which was connected to an isocratic pump, degasser and auto-sampler (Agilent 1200 series, Agilent Technologies). The separation channel was equipped with a short channel spacer (trapezoidal shape, height 350 µm, length 174 mm and largest width 21 mm). Membranes of regenerated cellulose (molecular weight cut off 5 kDa) were used as accumulation wall [20]. TRIS buffer was used as carrier liquid and for sample dilution. 20 µL of diluted samples (1 mg/mL GMO/Poloxamer) were injected (0.2 mL/min) and focused in the channel (focus flow 2 mL/min) for 5 min followed by elution at a fixed detector flow of 1 mL/min and subsequent cross flow gradients: Cross flow decreasing from 1 mL/min to 0.3 mL/min over 5 min and 0.3 mL/min to 0.05 mL/min over 30 min. A constant cross flow of 0.05 mL/min was then maintained over 10 min and finally elution was continued without applied cross flow for 10 min to facilitate complete sample elution. Size and size distributions were calculated by the Astra software version 4.90 (Wyatt Europe) applying the hollow sphere model. The average diameter is given by the Rw-value which is calculated by mass. Size distributions are presented by the characteristic diameters D10, D25, D50 (median), D75 and D90 [20]. The diameters are obtained by cumulative mass distribution. D10 means, for example, that 10% of the particles are smaller than the given diameter and 90% are larger.

2.8. Laser diffraction with PIDS instrumentation (LD-PIDS)

Size distributions of the formulations without diclofenac were also determined with a Beckman Coulter LS 13 320 which allows particle size measurements over a broad size range [22]. The measurements were carried out at the Institute of Pharmaceutical Technology (Prof. Heike Bunjes, University of Braunschweig, Germany). 100 to 200 µL of the 1:2 diluted samples were

injected into the instrument to obtain optimal PIDS signals (between 40 and 50%). 6 runs over 90 s each were carried out and results averaged. Size distributions by volume were calculated applying the Mie theory (refractive index of particles and dispersant were set to 1.45 and 1.33, respectively) by the LS Coulter software 4.03. Size distributions are presented by D10, D25, D50 (median), D75 and D90 as mentioned in the AF4/MALLS method.

2.9. Preparations of skin containing DiI stain

Skin obtained from the upper arm (female) was prepared. The subcutis tissue was removed in advance. Three skin pieces were cut to fit in the Franz cells. The receptor compartments were filled with TRIS buffer and the skin was clamped and 0.50 g of formulations applied (the stained formulations of dGMO_D3_7, dGMO_D0_8 and the diluted stock solution of DiI). The temperature in the receptor was set to 32°C which is the normal temperature of the skin [37] and the stirring of the Franz cells was 500 rpm (IKA® RO10). The donor compartments in the Franz cells were non-occluded and the formulations were allowed to penetrate the skin for 24 hours. Two small pieces of each skin containing formulation were cut and further prepared by cryo-sectioning. For cryo-sectioning, the skin sample was covered with mounting medium for cryotomy (O.C.T. compound, VWR Chemicals) in an aluminium basket. The aluminium basket was put in a metal beaker containing 2-methylbutane (Sigma-Aldrich) which was surrounded by liquid nitrogen. The basket was hold until the content was frozen and it was stored in a freezer (-80°C). The skin was sliced for investigations using a Cryotome FSE (Thermo Scientific) with a chamber temperature at -20°C. The skin was sliced perpendicular with a width of 20 µm of each skin sample (2 skin slices for each skin piece, 12 slices in total). The skin slice was placed on an object glass and covered with ProLong® Gold antifade reagent (molecular probes® by Life Technologies) and a cover slide.

2.10. CARS microscopy

The human skin (not containing any formulation or stain) was investigated by CARS microscopy. A cross section of the human skin (epidermis and dermis) was studied. The sample of the human skin was placed on an object glass and the skin was hydrated with 5 µL of Milli-Q water and covered with a cover slide. The cover slide was sealed with nail polish. The sample was viewed in a CARS microscope (Leica Microsystems SP8) through a 40x/1.10 water objective and the CARS signal detected with forward-CARS, epi-CARS, F-SHG and E-SHG and using the software Leica Application Suite X (LAS X) version 1.1.0.12420. The filters used in front of the detectors were a short pass 750 nm to block the laser followed by a 620/14nm for water, a 661/11nm for lipids and a 465/170nm for the SHG channel. All filters were purchased from AHF Analysentechnik AG, Tuebingen, Germany. To confirm that a CARS signal was seen one laser at a time (pump or Stokes) was turned off and the image would turn black. The laser light sources used was pico emirald (APE Berlin). The images were adjusted in (Fiji Is Just) ImageJ version 2.0.0-rc-48/1.50i.

2.11. Fluorescence microscopy

The skin preparations containing DiI stain were investigated by laser scanning confocal microscopy (Leica Microsystems) using the software Leica Application Suite X (LAS X) version 1.1.0.12420. The skin was viewed through a 100x/1.40 oil objective. The white light laser was turned on in a wavelength between 550 nm and 650 nm (according to the fluorophore DiI where light was emitted). The images were taken by Nyquist sampling and they were adjusted in (Fiji Is Just) ImageJ version 2.0.0-rc-48/1.50i.

3. Results

3.1. Size determination by DLS and light microscopy

The results from the size determination by DLS are shown in Figure 12 and 13. All data (both average values and the raw data) are summarized in Appendix II.

Particle sizes (DLS) of the formulations without diclofenac sodium (GMO_D0_4, GMO_D0_6 and dGMO_D0_8) and with 3% diclofenac decreased with increasing time of homogenization as expected (Figure 12). However, the diameter of the nanoparticles in the formulations containing only 1% diclofenac sodium (GMO_D1_3 and GMO_D1_5) became somewhat larger after centrifugation (30 minutes, Figure 12). The reason for this small size increase is unclear and needs further investigation.

The nanoparticles must be stable to be used as a formulation applied on skin and therefore the physical stability of the particles over time was measured (Figure 13). Interestingly, particle sizes slightly decreased over time (Figure 13). This is rather suspicious since it is expected that the particle sizes will increase or do not change over time. However, comparing size results obtained on day 10 and later time points, a minor increase was observed in all samples (Figure 13).

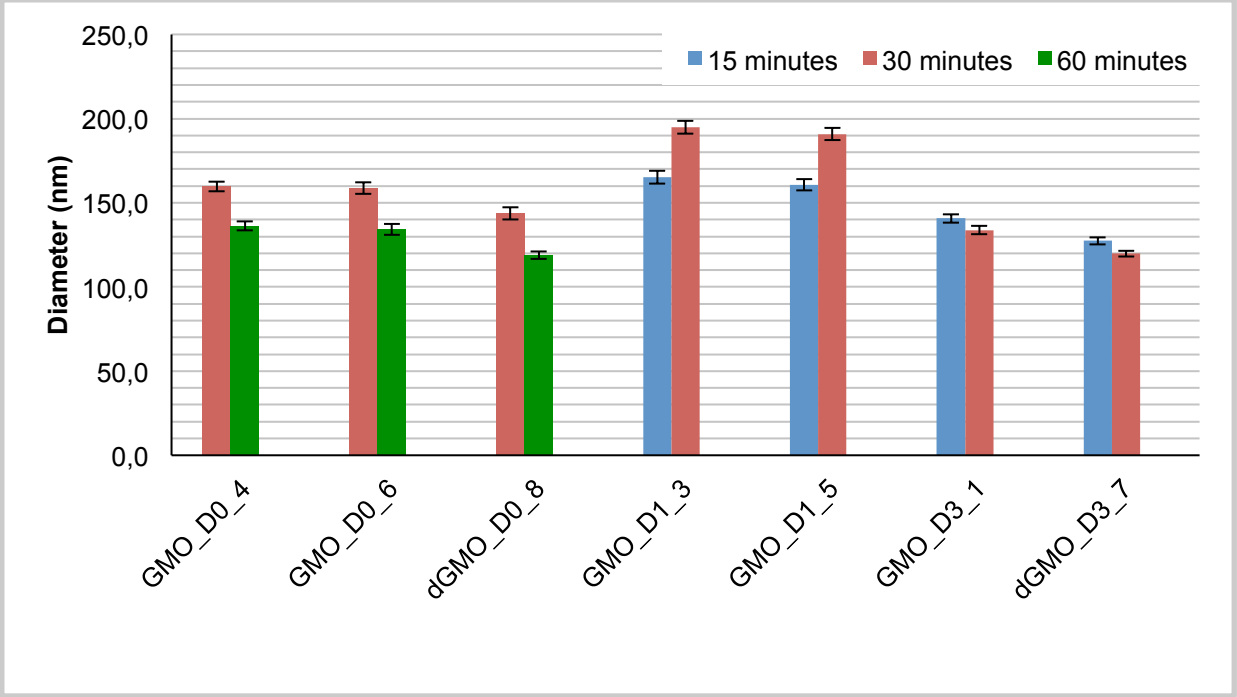

Figure 12: Hydrodynamic diameters by DLS (n = 4) of the nanoparticles 3 days after preparation together with their standard deviation (SD). GMO_D0_4, GMO_D0_6 and dGMO_D0_8 have been centrifuged for 30 minutes and 60 minutes, but GMO_D1_3, GMO_D1_5, GMO_D3_1 and dGMO_D3_7 for 15 minutes and 30 minutes. The average for the PDI values for the individual formulations are between 0.110 and 0.180 except dGMO_D0_8 which has a higher value of 0.225.

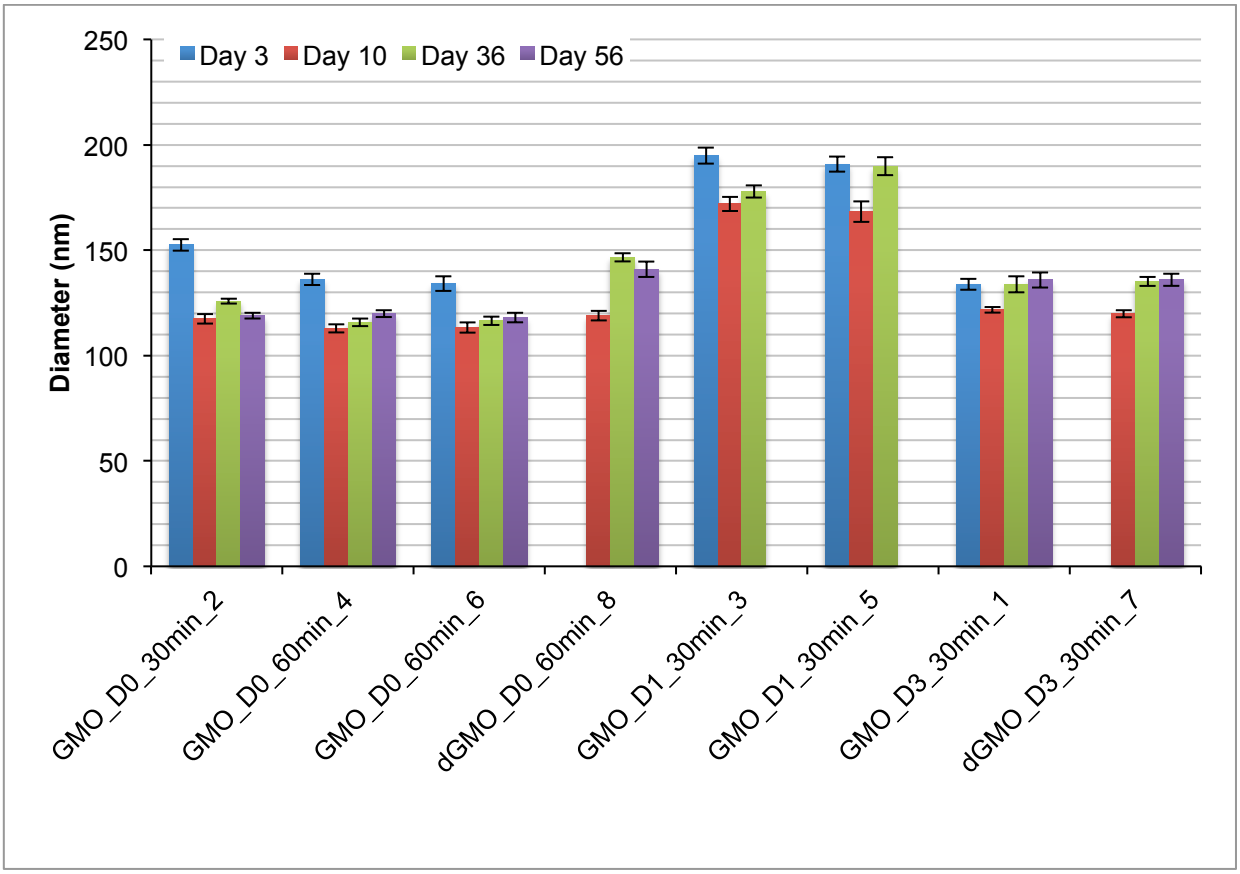

Figure 13: The hydrodynamic diameter by DLS (n = 2-4) of the nanoparticles measured at different time points together with their SD. The average PDI range for each individual formulation is between 0.120 and 0.220.

Upon visual inspection of the formulations without diclofenac sodium, a small precipitate was clearly detected. The smaller particle sizes determined at the later time points (day 10, 36 and 56) could be due to the lack of shaking prior size determinations. Therefore, the size determinations were repeated with samples where the sediment was carefully dispersed by manual shaking prior to size determination (Figure 14). The particles of the two formulations GMO_D0_60min_6 and dGMO_D3_30min_7 after shaking were larger than without shaking (seen at both day 36 and day 56) and a similar trend was seen for all measured samples (Appendix II, Figure A1). This indicates that re-dispersion of the sediment does influence the particle size results (DLS). Though, particle diameters were still smaller than the diameters obtained in the first measurements in most formulations (Appendix II).

All PDI values from the DLS measurements are given in Appendix II. A small value of PDI (<0.1) indicates a homogenous population and a higher PDI (>0.3) indicates a higher heterogeneity [33]. The PDI values measured for the nanoparticles are on average around 0.1-0.2.

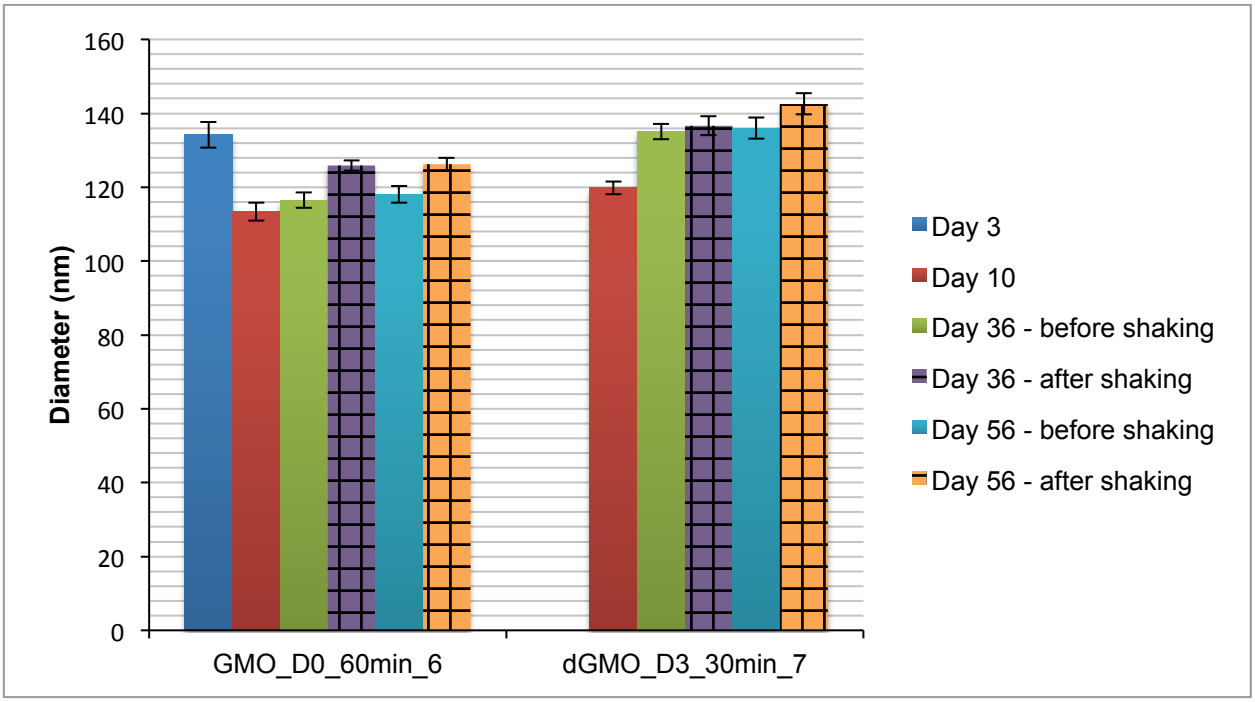

Figure 14: The hydrodynamic diameter (DLS) of the nanoparticles without and with shaking (squared) of the formulations prior measurements (GMO_D0_60min_6 and dGMO_D3_30min_7) together with their SD. There was the same tendency for all of the formulations with a small increase in the diameter after shaking (Appendix II, Figure A1).

DLS is only applicable for measuring particle sizes in the colloidal size range. Therefore the formulations were also examined by a light microscope to check for the presence of particles in the µm-size range. No particles were detectable in the formulations containing diclofenac sodium and hence only formulations without diclofenac sodium were investigated in more detail. A total of 50 pictures was taken for the formulations without diclofenac sodium after different centrifugation times (8 formulations in total, data not shown) and representative images are shown in Figure 15. In Figure 15 a), sample GMO_D0_2 with a centrifugation time of 15 min is shown. Some particles are 30 µm (30'000 nm) in diameter (and a few even larger) and there are several particles present with a diameter of 20 µm. In b) GMO_D0_30min_6 is seen and several particles with a diameter of around 5-10 µm are present. The centrifugation time compared to a) was doubled and the diameter of the largest particles decreased a lot. Figure 15 c) shows the same formulation as in b) but with the centrifugation time increased to 60 min. Some larger particles are still left but the amount has decreased distinctly. Overall, it is seen that the large particles present decrease distinctly in size after longer centrifugation time which is desirable for the formulations.

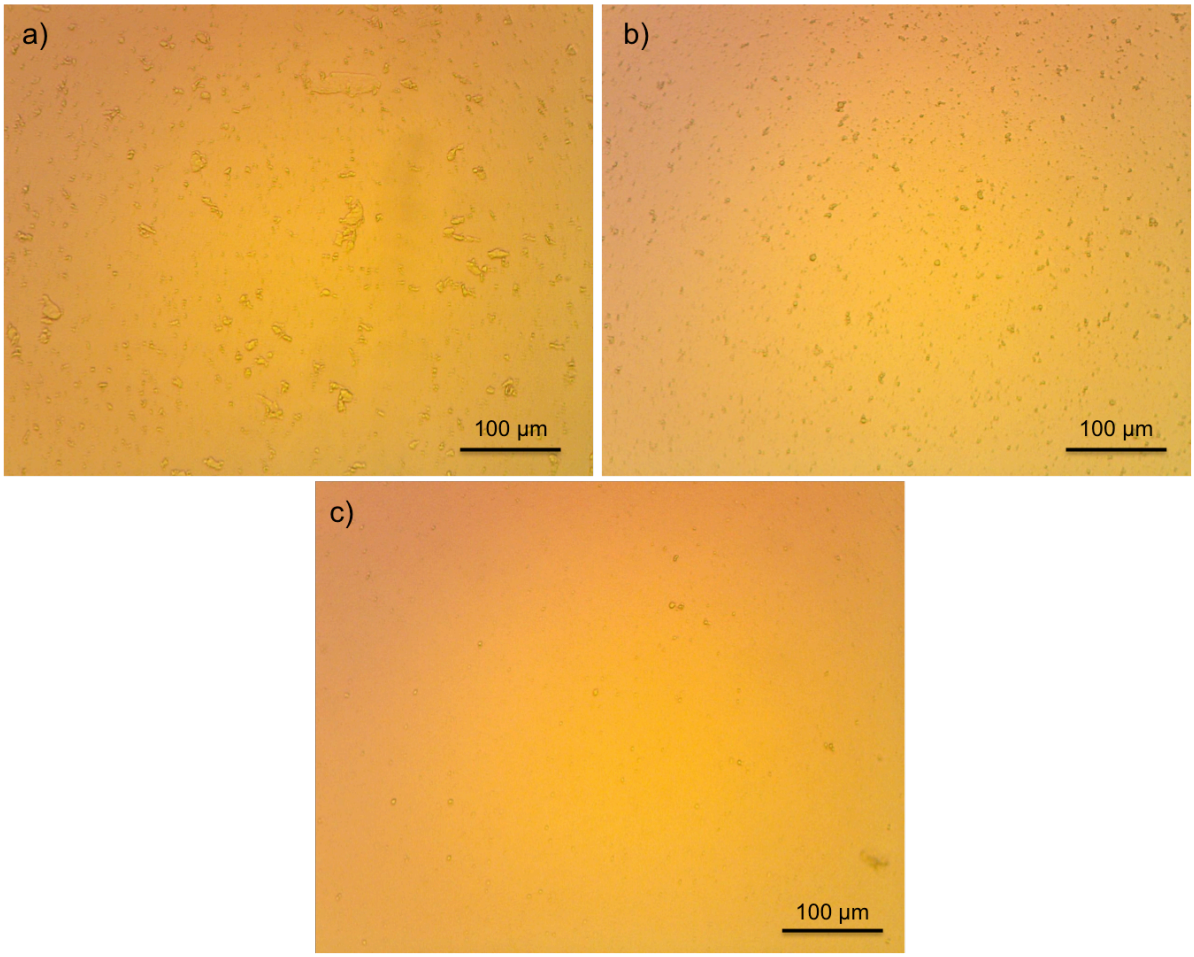

Figure 15: Representative light microscopic images (20x) of the formulations. a) GMO_D0_15min_2. b) GMO_D0_30min_6. c) GMO_D0_60 min_6.

3.2. Size determination by AF4/MALLS and LD-PIDS

The results obtained by AF4/MALLS are summarized in Table 4.

Table 4: The average size distribution in diameter ± SD (n = 3) obtained by AF4/MALLS.

Formulation	D10 (nm)	D25 (nm)	D50 (nm)	D75 (nm)	D90 (nm)	Mean (nm)
GMO_D0_60min_4	27.6 ± 4.3	34.5 ± 4.4	42.4 ± 3.6	52.5 ± 4.3	102.9 ± 11.1	223.5 ± 11.4
dGMO_D0_60min_8	31.4 ± 2.1	34.9 ± 1.4	38.7 ± 1.2	43.9 ± 1.6	69.2 ± 3.9	175.8 ± 7.2
GMO_D1_30min_3	57.9 ± 16.4	76.3 ± 17.4	102.3 ± 23.0	129.9 ± 26.2	154.4 ± 26.8	155.7 ± 5.5
GMO_D1_30min_5	46.3 ± 2.7	68.2 ± 2.8	96.2 ± 3.3	130.4 ± 3.9	159.3 ± 3.4	165.7 ± 2.1
GMO_D3_30min_1	28.8 ± 3.4	43.6 ± 4.5	61.9 ± 4.3	80.3 ± 4.1	98.4 ± 2.6	165.8 ± 13.3
dGMO_D3_30min_7	55.6 ± 2.3	66.2 ± 2.0	84.3 ± 1.9	104.8 ± 1.8	120.2 ± 2.0	165.4 ± 2.8

Figure 16 shows the elution profiles and size distributions of representative measurements for all formulations. The elution profile in a) shows that the particles start to be eluted around 20 min. The diameter of the eluted particles increase over elution time which is in good agreement with the principle of AF4 separation where the small particles elute earlier. This was similar for all the measured samples. Around 20 min signals from the light scattering are detected due to the elution of particles. From the formulation without diclofenac sodium, it is already seen that a larger fraction of small particles are being eluted which is consistent with the small D10 values in Table 6 for the formulations without diclofenac compared to the diclofenac-loaded particles. Around 60 min the final elution (without applied cross flow) happens and all particles are being eluted showing that there are still some particles left in the formulation without diclofenac sodium. From the laser scattering signals, the size distributions in b) are obtained. In good agreement with DLS results, larger mean sizes were detected for formulations without diclofenac sodium. Interestingly, size distribution was bimodal with maxima at around 40-50 and 300-400 nm. In contrast, monomodal size distributions were obtained for the diclofenac-loaded nanoparticles with smaller particles with increasing diclofenac load. The same trend is seen for the deuterated formulations both with and without diclofenac sodium in c) and d). Overall, there is a good agreement of all results.

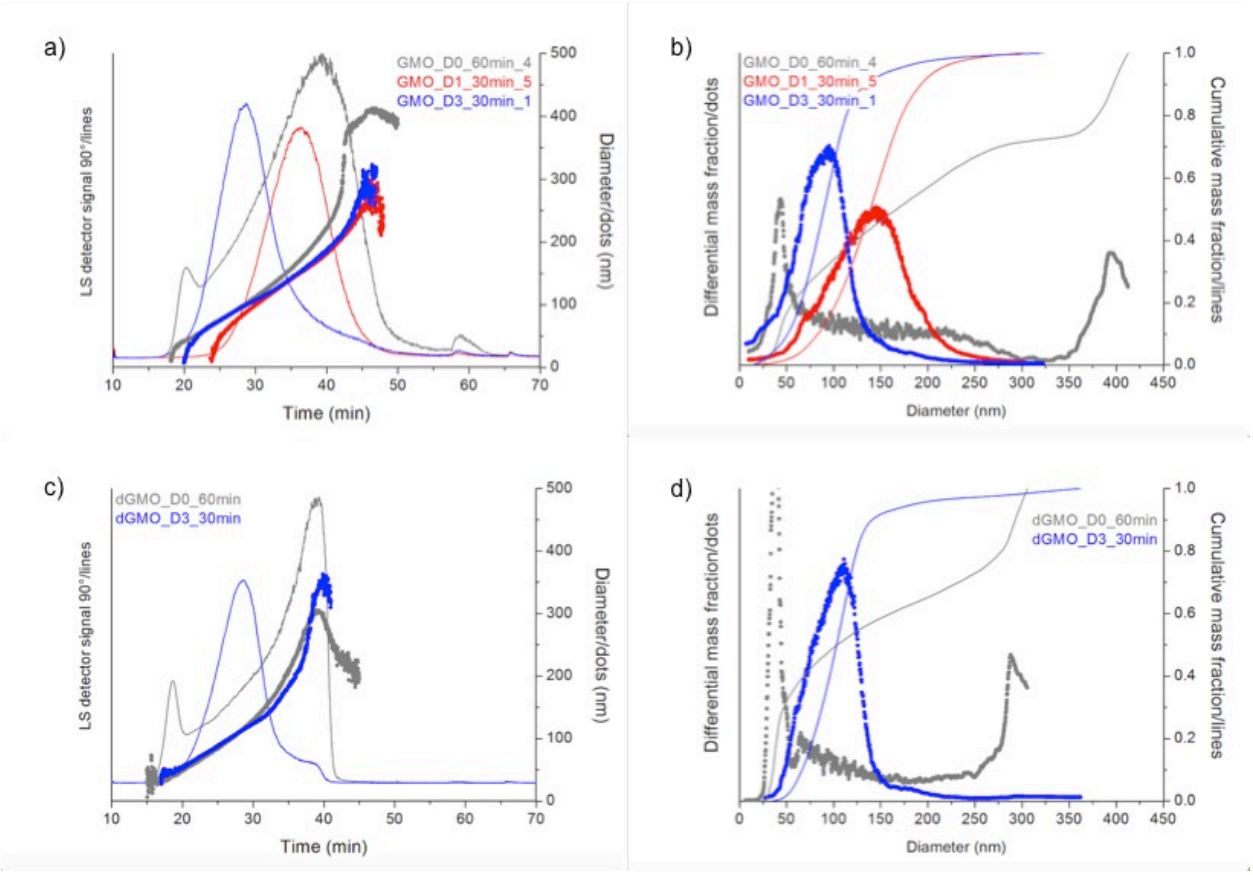

Figure 16: Size distribution of five formulations obtained by AF4/MALLS. a) and b) GMO_D0_60min_4, GMO_D1_30min_5 and GMO_D3_30min_1, c) and d) dGMO_D0_60min_8 and dGMO_D3_30min_7. In a) and c) the dots show the diameter (nm) as a function of time (min) and the lines show the LS detector signal 90° as a function of time (min). In b) and d) the dots show the differential mass fraction as a function of the diameter (nm) for each formulation and the lines show the cumulative mass fraction as a function of the diameter (nm).

Finally, particle sizes of drug-free formulations were measured by LD-PIDS at the University of Braunschweig (Table 5). Here it is observed that a shorter centrifugation time (GMO_D0_30min_2) shows a broader size distribution (also seen by the mean diameter, Table 5).

Table 5: The size distribution of non-loaded cubosome dispersions obtained by LD-PIDS. The distribution is given as the average of 6 measurement runs (individual data not provided).

Formulation	D10 (nm)	D25 (nm)	D50 (nm)	D75 (nm)	D90 (nm)	Mean (nm)
GMO_D0_30min_2	113.7	178.7	328.7	1304.3	2068.0	2739.7
GMO_D0_60min_4	75.0	96.0	132.0	194.0	299.0	164.0
GMO_D0_60min_6	79.0	103.0	150.0	239.5	370.5	202.0
dGMO_D0_60min_8	79.0	103.0	150.0	235.0	356.0	187.0

The size distribution as a volume fraction (%) as a function of the diameter is shown for both GMO_D0_30min_2 and GMO_D0_60min_4 in Figure 17. A fraction of very large particles (around 10-100 µm) were observed in the dispersion obtained after 30 min of centrifugation. Longer centrifugation time (GMO_D0_60min_4) resulted in a monomodal size distribution. For the other formulations without diclofenac sodium with a centrifugation time of 60 min the size distribution is almost equal with D10, D25, D50, D75 and D90 values which are almost the same (Table 5).

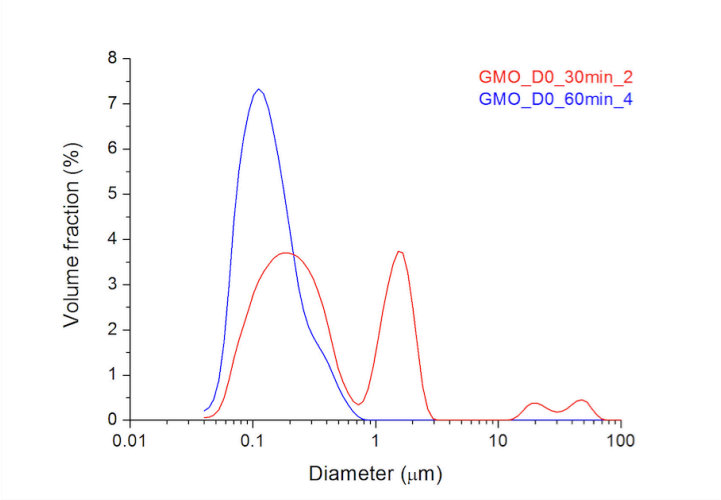

Figure 17: Size distribution for GMO_D0_30min_2 and GMO_D0_60min_4 obtained by LD-PIDS. The volume fraction (%) as a function of diameter (µm) is shown.

3.3. Investigations of skin structure and prepared formulations by CARS and fluorescence microscopy

14 images of the skin were taken in total in the CARS microscope and representable images are shown in Figure 18. Figure 18 a), b) and c) show cross sections of the skin whereas Figure 18 d) shows the surface of the skin. In Figure 18 a), the red color shows the visualization of the lipids in the skin. The different cell layers in stratum corneum are seen and the cell contour in the rest of the epidermis is visible whereas the cells in the dermis are more blurred. In Figure 18

b), the green color visualizes the collagen which is seen in the dermis, as expected. Figure 18 c) shows an overlay of Figure 18 a) and b) and the different parts of the skin (SC, epidermis and dermis) are named. In Figure 18 d) the blue color visualize water on the skin. The darkest areas seen are due to the morphology of the skin surface [38] and in these areas water has not penetrated.

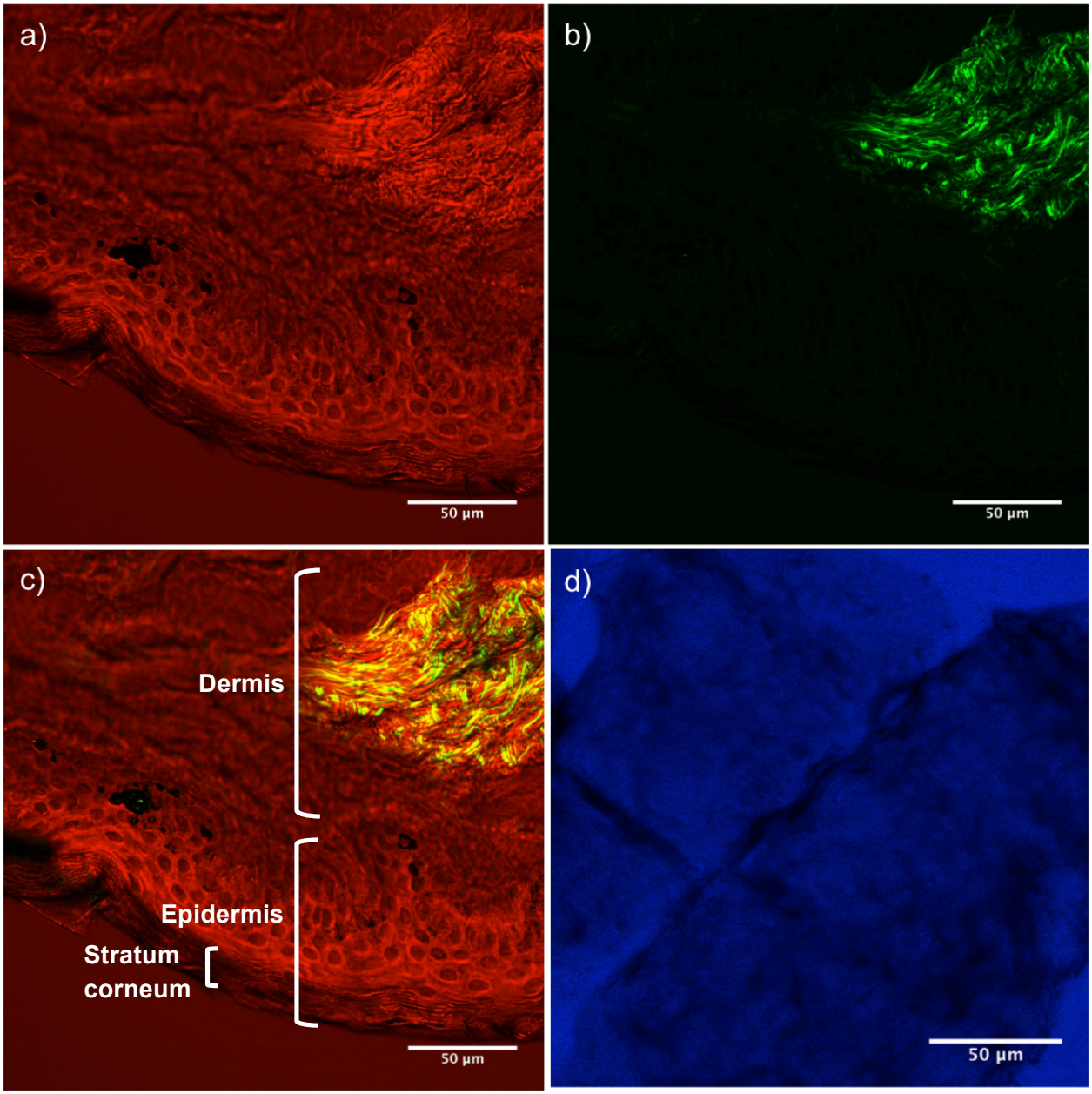

Figure 18: Representative CARS microscopic image of the skin. a) The visualization of the lipids in the skin. The wavenumber investigated for the lipids is 2100 cm^{-1}. b) Collagen visualized by the SHG detectors. c) Both the lipids and the collagen are visualized (composite of the images above). d) Water on the skin surface. The wavenumber investigated for water is 3400 cm^{-1}.

A spectrum of the intensities as a function of the wavelength of the pump laser can be made for an investigated compound. The spectrum of two of the investigated formulations (GMO_D0_30min_2 and dGMO_D0_60min_8) and deuterated glucose are shown in Figure 19. A characteristic vibrational energy for CD bonds are expected at 2100 cm^{-1} [30]. This can be

converted to a wavelength for the pump laser due to the non-tunable Stokes laser (at 1064 nm) with the formula (given by the software LAS X):

$$\tilde{v}_{vib} = \frac{1}{\lambda_{pump}} - \frac{1}{\lambda_{Stokes}}$$

The wavelength can then be calculated:

$$2100\ cm^{-1} = \frac{1}{\lambda_{pump}} - \frac{1}{1064\ nm} \Leftrightarrow \frac{1}{\lambda_{pump}} = \frac{2100\ cm^{-1}}{1 \cdot 10^{7}\ \frac{nm}{cm}} + \frac{1}{1064\ nm} \Leftrightarrow$$

$$\frac{1}{\lambda_{pump}} = 0{,}001149\ nm^{-1} \Leftrightarrow \lambda_{pump} = 870\ nm$$

A strong signal is expected at 870 nm in the deuterated formulation due to the CD bond. When comparing the formulations prepared (GMO_D0_30min_2 and dGMO_D0_60min_8) the intensities measured are quite high especially for the deuterated formulation (Figure 19). A signal is seen in the interesting wavelength in the deuterated formulation but the same signal is also present in the non-deuterated formulation where nothing is expected to be seen. The intensity between the two peaks do not differ much. Other signals are seen at the same wavelengths in both formulations (e.g. at 870.9 and 864.7 nm) but there are no strong signals which easily can be identified due to the high intensities in general. A control sample (deuterated glucose) was investigated, where it is seen that the signal at 870 nm is strong as expected unlike the signal in the deuterated formulation. A high intensity of the individual investigated signal in the formulation is desired and these results can be due to the signal being too weak because of the number of deuterated atoms are too low and therefore more CD bonds are needed. The results can also be due to the non-resonant background from the samples.

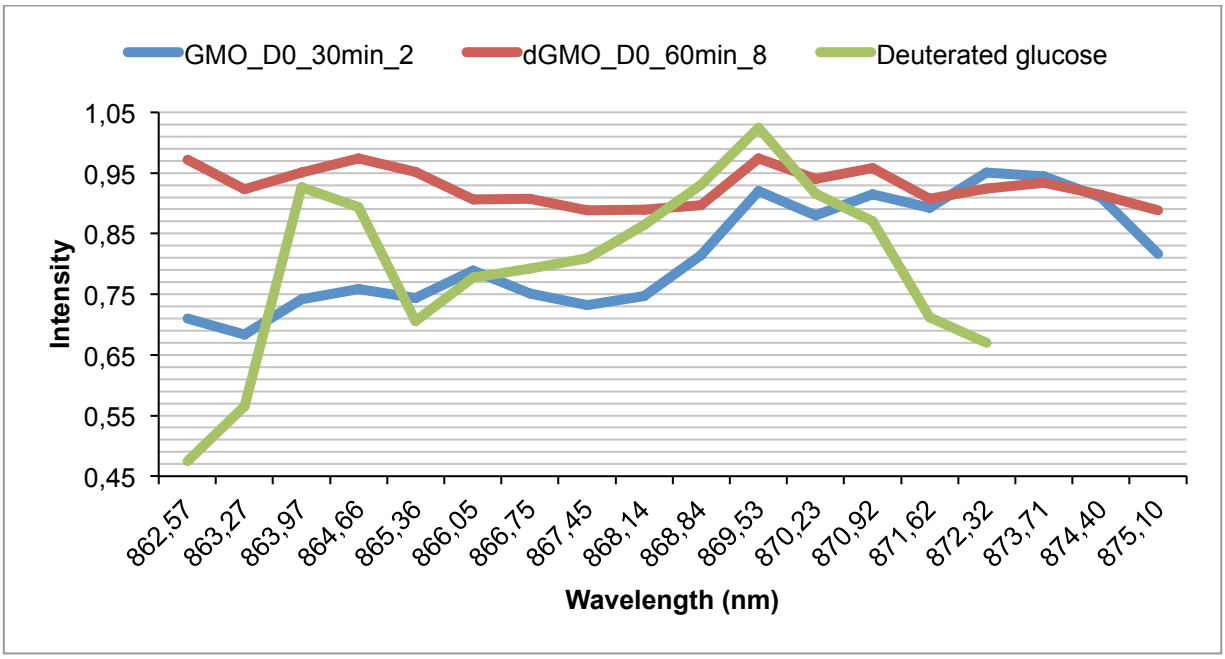

Figure 19: The spectrum of GMO_D0_30min_2, dGMO_D0_60min_8 and deuterated glucose obtained from CARS microscopy. The figure shows the intensity as a function of pump laser wavelength. Data have been normalized. At 870 nm the signal from the CD bond is expected and is clearly seen in the deuterated glucose.

Due to the weak signal in the CARS microscope, the deuterated formulations (dGMO_D0_60min_8 and dGMO_D3_30min_7) were labeled with the fluorophore, DiI, for the purpose of investigating the penetration of the formulations into skin in a fluorescence microscope. To make sure that the ethanol from the stock solution does not alter the particle sizes in the formulations, the particle sizes of the stained formulations were measured by DLS. The results show that the particle sizes were similar after adding the DiI stock solution containing ethanol to the particle sizes from day 56 (the last measurement made of the particle sizes without stain, see Appendix II, Table A4 and Figure A2). The particle sizes after re-dispersion of the sediment (shaking) were similar to the particle sizes before shaking in the stained formulations.

Representative images of the investigated stained formulations can be seen in Figure 20. The red color is visualizing the stained nanoparticles. Some larger particles are present in the formulation without diclofenac sodium shown in Figure 20 a) compared to the diclofenac-loaded formulation in Figure 20 b). This is in agreement with the former results from DLS and AF4/MALLS (Figure 13 and Table 4).

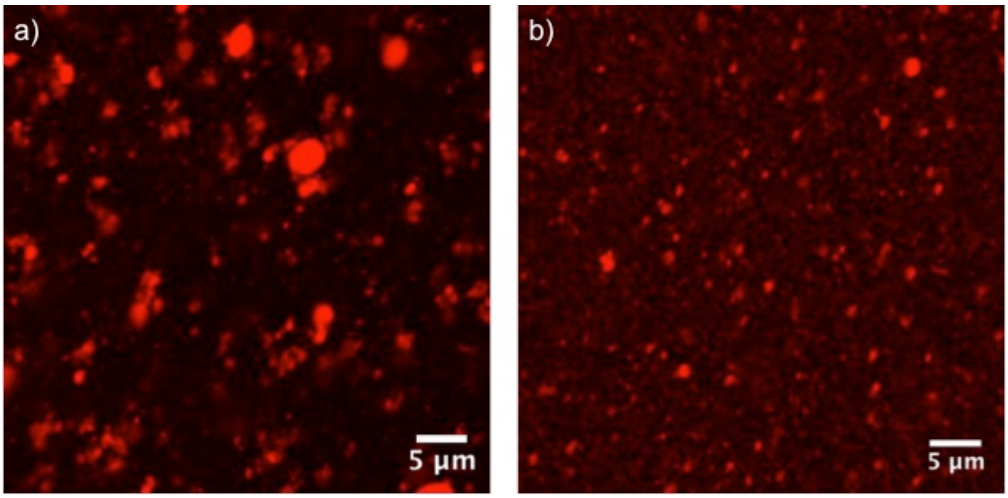

Figure 20: The investigated formulations stained with DiI viewed by the LSCM. The red spots in the images illustrate the nanoparticles. a) dGMO_D0_60min_8. b) dGMO_D3_30min_7.

Figure 21 shows fluorescence microscopic images of skin cross sections incubated with dGMO_D0, dGMO_D3 and a control solution containing DiI. By observing the same formulation (e.g. dGMO_D0_60min_8 in a), b) and c)) it is seen that the formulation did not penetrate equally all over the skin surface. This could be due to an unequal distribution of formulation on the skin in the Franz cells. Overall, it is seen that the formulation penetrated the skin deeper upon application of both dGMO_D0_60min_8 (Figure 21 a-c) and dGMO_D3_30min_7 (Figure 21 d-f) on skin. The DiI control solution (Figure 21 g-i) did not or just barely crossed the stratum corneum and mostly remained on the surface of the skin.

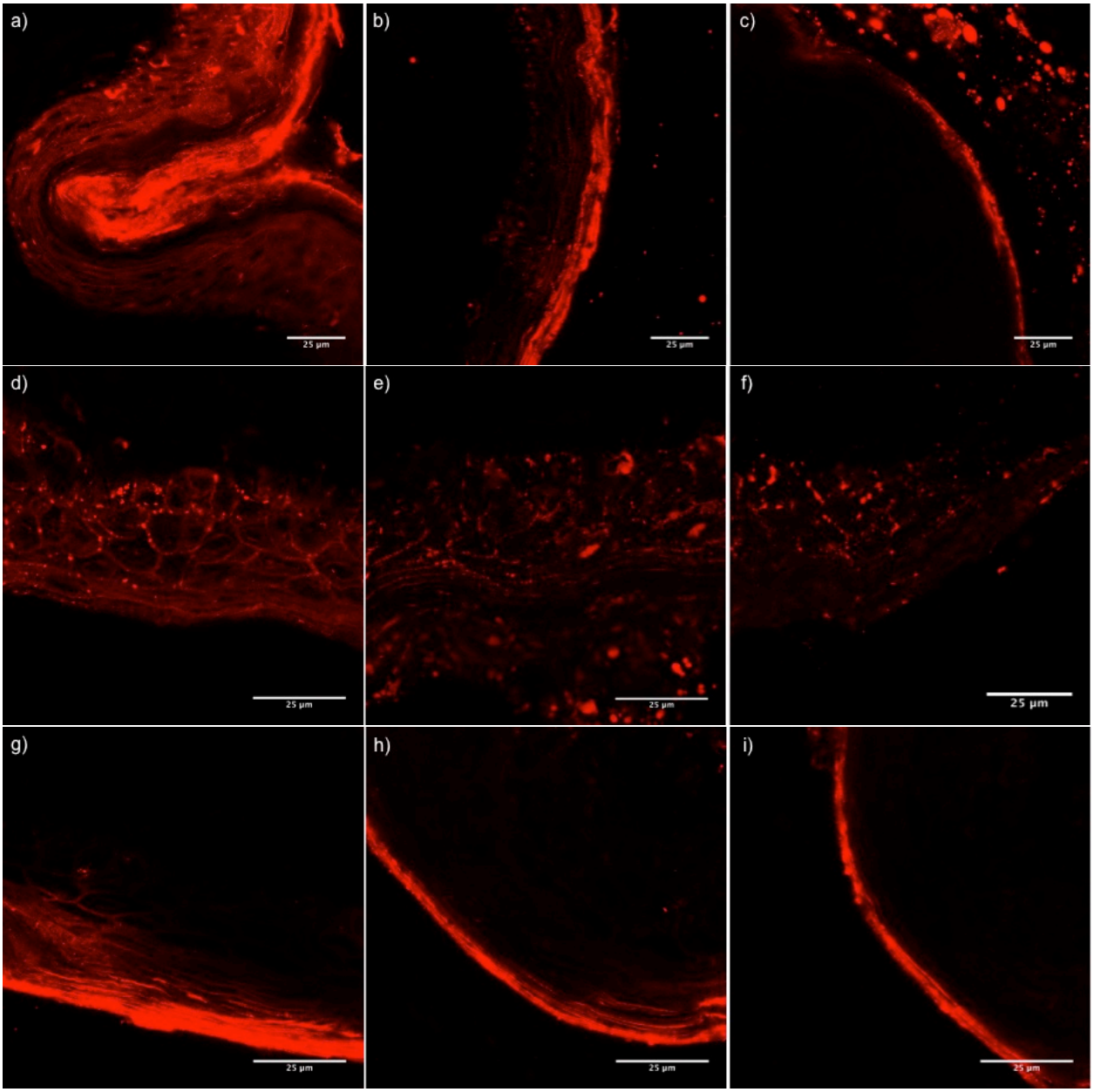

Figure 21: The different formulations applied on skin. a), b) and c) dGMO_D0_60min_8. d), e) and f) dGMO_D3_30min_7. g), h) and i) DiI control solution. The scale bar represents 25 µm.

In Figure 22, enlarged representative images of skin cross sections incubated with the different formulations are shown. The contrast has been adjusted from the images in Figure 21. In Figure 22 a) it is clearly observed that the formulation dGMO_D0_60min_8 penetrated the skin into the epidermis due to clusters in the deeper layers and also nanoparticle-like structures are observed. Though, more of the formulation dGMO_D3_30min_7 penetrated into epidermis as indicated by the higher intensity of the red color visualizing the DiI (Figure 22 b)). In Figure 22 c), the DiI control solution is seen. Even with a high contrast it is seen that most of the solution does not penetrate further than to the SC.

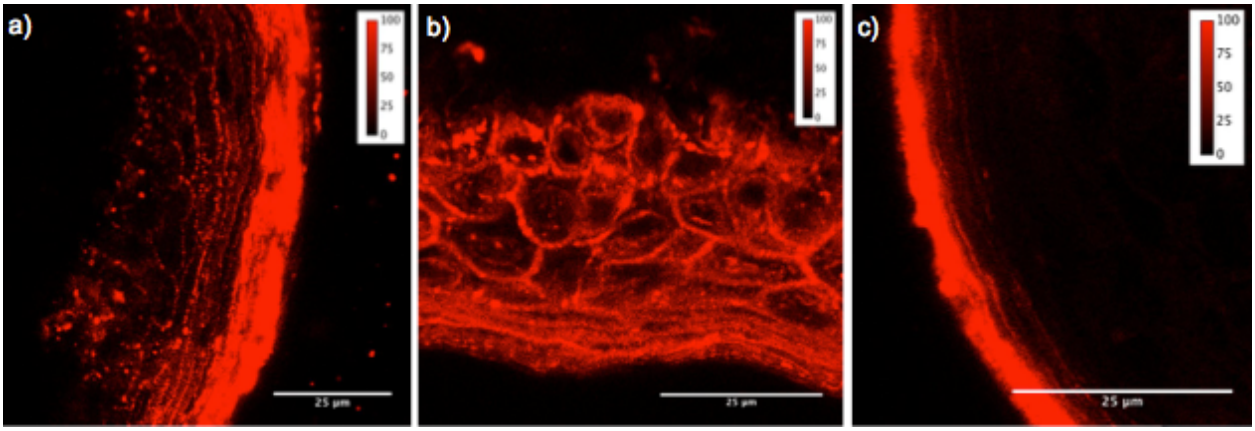

Figure 22: Enlarged and adjusted images from Figure 21 showing the penetration depth of the different formulations into the skin: a) dGMO_D0_60min_8. b) dGMO_D3_30min_7. c) DiI control solution.

4. Discussion

Due to the properties of cubosomes such as their bilayered structure, they are under investigation for different routes of administration including topical delivery [12]. The particle size is important in drug formulations and the diameter of the cubosomes has been measured by different methods in this study. The results from DLS (Figure 13) show that the particle sizes of all formulations were between 110 and 150 nm apart from the formulations containing 1% diclofenac sodium. The tendency is that the particle sizes decreased distinctly in the later measurement time points (e.g. storage time) which was not expected. This decrease could be explained by sedimentation of the larger particles over time. This could therefore be avoided by re-dispersion of the sediment prior to measurement. The deuterated formulations both had a diameter of around 120 nm and particle sizes slightly increased over time as expected in the DLS measurements. Though, in the formulation without diclofenac sodium, the particle size increased slightly more over storage time compared to the formulation containing diclofenac sodium. Moreover, AF4/MALLS measurements revealed a larger mean diameter of the deuterated formulation without diclofenac sodium than the formulation containing diclofenac sodium indicating a larger amount of large particles to be present in the deuterated diclofenac-containing formulation. The tendency was that all the mean sizes determined by LD-PIDS and AF4 were higher than the results obtained from DLS. This could be because of DLS only measuring the small particles and therefore the average will be lower. The DLS cannot measure particles in the larger size range (µm-size range) and some of the smaller particles in the formulation will not be measured due to too much light being scattered from the bigger particles in the sample as the light scattering strongly depends on particle size. However, the presence of larger particles (µm-size range) has been observed in a light microscope. In the GMO_D0_30min_6 formulation particle diameters of 5-10 µm are observed whereas the same centrifugation time (GMO_D0_30min_2) measured by LD-PIDS reveals larger particle sizes (50 µm and larger). This size difference is possibly because of the volume of sample investigated in respectively LD-PIDS and in the light microscope. A much smaller volume was investigated in the light microscope (one drop) compared to the volume investigated in LD-PIDS (100 to 200 µL). Therefore, by investigating more samples from the same formulation quantitatively in the light microscope more large particles would probably be seen.

In the present study, formulations have been prepared by dual centrifugation. The time of centrifugation influences the particle sizes [17] which is clearly seen in the light microscope and from DLS and LD-PIDS measurements too. When increasing the centrifugation time from 30 minutes to 60 minutes, the particle size decrease distinctly (the mean particle size measured by DLS, the bigger particles in the µm-range seen in the light microscope and the size distribution measured in LD-PIDS). From the LD-PIDS measurements it is seen that GMO_D0_30min_2 had a much broader size distribution with an average diameter above 2700 nm compared to the formulations centrifuged for 60 min which had much smaller average diameters of around 200 nm. This decrease in size by increasing centrifugation time from 30 minutes to 60 minutes is worth noticing in comparison to other studies with liposomes [17] where it is found that longer centrifugation time than 30 minutes does not decrease the mean particle size anymore. This statement can be due to different structures (liposomes) or the centrifugation speed where the speed was set to 3540 rpm whereas in this paper cubosomes have been prepared at a centrifugation speed of 2500 rpm. A decrease in the centrifugation speed will result in increased sizes and a broader size distribution [17]. An increase in the centrifugation speed could be

checked with the cubosome formulations, but with the used speed of 2500 rpm a higher centrifugation time was necessary to prepare smaller cubosomes.

The PDI values obtained from DLS were between 0.1 and 0.2. These are quite good results and show that the formulations contain almost a homogenous population. Though, all results (including AF4 and LD-PIDS) are calculated from the sphere model even though cubosomes are not spherical particles. The advantage of DLS compared to LD-PIDS and AF4 is that it can give measurement results fast (60 sec) where LD-PIDS and AF4 is slower in measuring the sizes (9 min and 70 min respectively). A disadvantage of DLS is that it has to be supported by light microscopy since it is not able to measure particles in the µm-size range (which are present, Figure 15). The z-average will therefore be lower when larger particles are not included in the calculations. Furthermore, DLS will only give an average diameter of the particles whereas the advantage of both LD-PIDS and AF4 is that they can provide a size distribution and measure both smaller and larger particles. Though, LD-PIDS cannot measure particle sizes less than 40 nm which AF4 is able to. In some of the formulations measured by AF4, it is seen that the D10 value is less than 40 nm meaning that 10% of the particles are smaller than the given diameter. Compared to LD-PIDS the D10 value is 75 nm and above. This higher D10 value is probably due to the small particle sizes which were not detected by LD-PIDS (out of measurement range). Furthermore, the size distribution of GMO_D0_30min_2 shows diameter values where the volume fraction is zero, meaning that no particles in this size range are measured (Figure 17). This is not expected since larger diameters around 10 to 100 µm in the same measurement are obtained.

When preparing cubosomes, it should be checked that the particles actually have a cubic structure since other structures (as vesicles, Figure 2) can be formed too. This has not been done in this project and therefore, it is not certain if the formulations prepared actually contain cubosomes. Though, since particles were measured in all three size determining methods particles are definitely formed but these can have different structures which need to be clarified. To investigate the morphology of the formulations they should be measured with small angle X-ray scattering and/or viewed in a cryo-electron microscope which would be able to tell if the particles are cubosomes or have another morphology [10].

CARS microscopy can be used to directly visualize the skin and other structures without any staining as different vibrational energies of the bonds in lipids and other molecules are known and used for visualization (Figure 18). Deuterium has been used in the formulations to distinguish between the CH bonds in the lipids of the skin and the CD bonds in the lipid chains in GMO. Though, the CD bond which was expected to be seen clearly with the pump laser at 870 nm was not clearly detected as opposed to the signal from the CD bond in the control sample of deuterated glucose. This can be due to the non-resonant background which is measured or because of the lack of CD bonds and therefore the signal is not high enough. Due to these issues the formulations were stained with DiI for further investigation in fluorescence microscopy. When using the LSCM the dye (due to known wavelength of emission) and hence the influence of the nanoparticles of DiI penetration are easily detected both when the formulation is investigated alone and when applied on skin (Figure 21 and 22). By observing the formulations in LSCM it is seen that some larger particles are present in dGMO_D0 than in dGMO_D3 which is detected in the measurement by AF4/MALLS as well where dGMO_D0 show a bimodal size distribution.

As investigated in another project with cubosomes [39] the formulations in this project penetrated the skin too (Figure 21). Though, the formulations did not penetrate equally all over the skin surface which can be due to uneven application of the sample on the skin. When the skin was clamped in the Franz cells, it would bend due to the buffer beneath and the formulation would gather in the “corners” of the donor compound. Therefore, the skin would be exposed to more formulation in the “corners” than in the middle of the skin in the setup and the penetration in the corners would probably be higher (in the dispersion dGMO_D0 and in the DiI control solution compared to dGMO_D3 with a gel-like structure). When cutting the skin samples in the cryo-microtome, the distribution of the formulation would not be equal in all samples since it depended on where on the skin the piece was sliced. Some skin samples were destroyed due to the SC being separated from the underlaying tissue (data not shown). This might be prevented by slicing cross sections thicker than 20 µm (as it has been done in this project). Though, the cross sections should not be too thick due to the limitation of the laser scanning confocal microscope (depth of 100 µm [26]). The penetration of the investigated formulations were studied along the SC and were mostly seen in the microscope as represented in Figure 22. The formulation dGMO_D0 penetrated into the epidermis but not as much as dGMO_D3 as is seen when comparing the intensities. In the formulation without diclofenac sodium a high intensity is obtained in SC indicating that a lot of the formulation has gathered in the SC. In dGMO_D3 the intensity of the SC is lower but a higher intensity throughout the epidermis with more nanoparticles/DiI are obtained in this formulation compared to the formulation without diclofenac. A reason for this can be that the diclofenac containing formulation is a gel and has a higher viscosity compared to the formulation without diclofenac sodium (which is a dispersion) and therefore it is easier to distribute equally on the skin. Most places where the skin with dGMO_D3 was applied would therefore apparently penetrate as deep as illustrated. For further penetration of both formulations and for a more equal distribution in the epidermis of the formulation without diclofenac it would be interesting to let the Franz cells experiment run for longer than 24 hours.

When comparing the DiI control solution on skin a clear difference is seen from the formulations containing nanoparticles. The DiI has gathered in the SC (a very strong intensity seen) and only a little has penetrated. A possibility of some of the intensities seen in the investigated skin slices can be due to contamination when slicing the skin in the cryo-microtome apparatus. When slicing the skin some of the formulation from the surface of the skin (applied on SC) could be “moved” down through the skin with the knife. Though, especially in the skin where dGMO_D3 was applied, a clear structure of the skin is seen and this cannot be due to contamination but due to the penetration effect. Contamination is seen as red spots and it is still possible that some of the strong intensities seen is because of this. However, when observing the penetration of the formulations it is possible that some of the intensities seen are due to the free DiI and not just the nanoparticles themselves.

The penetration enhancing effect can be due to the cubic structure of the particles (though, the structure should be investigated as mentioned since morphology influences penetration) but GMO has a skin-penetrating effect itself which can have an influence. The small amount of DiI from the DiI control solution which have penetrated can be due to the ethanol which also has a penetration enhancing effect on skin. Ethanol is found in both formulations as well (with a smaller volume compared to the DiI control solution) but the penetration enhancing effect will be comparable between the two formulations because of the same volume of ethanol. The particle size may also have an influence and in the formulation where the penetration is higher

(dGMO_D3) there are fewer large particles present as compared to dGMO_D0. The D90 value obtained from AF4/MALLS for the particles is around 70 nm with a mean size of 175 nm and for the diclofenac-loaded formulation the D90 value is 120 nm with a smaller mean size (165 nm). In studies with liposomes [33] the size of the particles are seen to influence the penetration where smaller particles penetrate deeper as is the case in this study with cubosomes.

There are advantages and disadvantages by use of both CARS and LSCM. When using CARS, dyes are avoided due to the contrast which is based on the molecular vibrations and the sample will in this way remain almost unaffected when investigated and we get to study the sample and not just a dye. Dyes are used for the visualization in LSCM and over time they bleach and lose intensity and can alter the sample [29]. CARS allows imaging in thick tissues (up to 0.4 mm depending on the wavelength [30]) and LSCM only allow imaging of thin sections up to 100 µm in thickness [26]. In this project, it was found that the CARS microscope did not have enough sensitivity to image the deuterated samples. However, the samples were easily visualized using the fluorescent dye DiI and LSCM. The signal in the CARS measurements could have been improved by using more deuterated lipids in the sample.

5. Conclusions

Formulations containing cubosomes (GMO nanoparticles) and the active ingredient diclofenac sodium have been prepared. However, to be certain about the cubic structure, measurements with small angle X-ray scattering should be performed and/or the samples should be viewed in a cryo-electron microscope. Different results were obtained from different size determining methods and due to limitations of each method there is not any single method which can provide the “correct” size of the particles. Combining the different methods, however, provide good information of particle size and particle size distributions.

The skin and the formulations have been investigated by CARS microscopy. The skin was easily visualized but signals from the formulations were difficult to obtain. No clear signal from the CD bonds in the deuterated formulations were detected and therefore preparing a formulation containing a higher amount of deuterated GMO could be worth doing and investigating by CARS.

The prepared formulations have been stained with DiI with the purpose of investigating the penetration of them on skin. The nanoparticles penetrated the epidermis and by extending the diffusion cell experiment they might penetrate even deeper. Furthermore, in the interest of the delivery of the active ingredient to the site of action the amount of diclofenac sodium the nanoparticles contain should be investigated. The penetration of the prepared nanoparticles could also additionally be compared to the penetration of liposomes or other lipid nanoparticles.

In conclusion, GMO nanoparticles do penetrate the skin and function as an enhancer both with and without the active ingredient as is clearly seen by comparing the fluorescence microscopic images of the samples to the DiI control solution on skin. The formulation containing diclofenac sodium showed a stronger penetration enhancement in the epidermis compared with formulations without diclofenac sodium. This could be due to the smaller size of the particles. However, more investigations are necessary to elucidate the mechanism of penetration enhancement.

Acknowledgement

This bachelor project was carried out at the Department of Physics, Chemistry and Pharmacy and at Memphys at the University of Southern Denmark, Odense.

I would like to thank Professor Heike Bunjes at the University of Braunschweig, Germany, for carrying out the measurements of LD-PIDS. I thank the Odense University Hospital for providing skin samples for the in vitro experiment carried out with Franz cells. Furthermore, I want to give thanks to Irina Antonescu for introduction and help with the experiment with Franz cells. For help with the fluorescence microscopy I thank Bjarne Thorsted. At last, I want to thank my advisors Judith Kuntsche and Jonathan Brewer for all of their help and guidance during this project.

References

1. Banga, A.K., *Transdermal and Intradermal Delivery of Therapeutic Agents: Application of Physical Technologies*. 2011: CRC press. p. 10-18.
2. Prausnitz, M.R. and R. Langer, *Transdermal drug delivery.* Nature Biotechnology, Volume 26, Number 11, 2008: p. 1261-1267.
3. Menon, G.K., *New insights into skin structure: Scratching the surface.* Advanced Drug Delivery Reviews 54 Suppl. 1, 2002: p. S3-S17.
4. Marieb, E.N., P.B. Wilhelm, and J. Mallatt, *Human Anatomy*. Seventh ed. 2014: Pearson Education. p. 124-130.
5. Schuenke, M., E. Schulte, and U. Schumacher, *Atlas of Anatomy: General Anatomy and Musculoskeletal System*. 2006: Thieme Medical Publishers. p. 328.
6. Williams, M.L. and P.M. Elias, *From Basket Weave to Barrier.* Arch. Dermatol. 129, 1993: p. 626-628.
7. Brown, M.B., et al., *Dermal and Transdermal Drug Delivery Systemt: Current and Future Prospects.* Drug Delivery 13, 2006: p. 175-187.
8. Florence, A.T. and D. Attwood, *Physicochemical Principles of Pharmacy*. Fifth ed. 2011: Pharmaceutical Press. p. 221-227.
9. Esposito, E., et al., *Cubosome Dispersions as Delivery Systems for Percutaneous Administration of Indomethacin.* Pharmaceutical Research, 2005: p. 2163-2173.
10. Kuntsche, J., et al., *Interaction of lipid nanoparticles with human epidermis and an organotypic cell culture model.* International Journal of Pharmaceutics 354, 2008: p. 180-195.
11. Wörle, G., et al., *Influence of composition and preparation parameters on the properties of aqueous monoolein dispersions.* International Journal of Pharmaceutics 329, 2007: p. 150-157.
12. Karami, Z. and M. Hamidi, *Cubosomes: remarkable drug delivery potential.* Drug Discovery Today, Volume 00, Number 00, 2016: p. 1-13.
13. Wörle, G., et al., *Transformation of vesicular into cubic nanoparticles by autoclaving of aqueous monoolein/poloxamer dispersions.* European Journal of Pharmaceutical Sciences 27, 2006: p. 44-53.
14. Bender, J., et al., *Lipid cubic phases for improved topical drug delivery in photodynamic therapy.* Journal of Controlled Release 106, 2005: p. 350-360.
15. *Produktresumé for Voltaren, gel*. 13/04-2016; Available from: http://www.produktresume.dk/docushare/dsweb/GetRendition/Document-22606/html.
16. *Produktresumé for Solaraze, gel*. 13/04-2016; Available from: http://www.produktresume.dk/docushare/dsweb/GetRendition/Document-18129/html.
17. Massing, U., S. Cicko, and V. Ziroli, *Dual asymmetric centrifugation (DAC) - A new technique for liposome preparation.* Journal of Controlled Release 125, 2008: p. 16-24.
18. *Malvern technical note: Dynamic light scattering: An introduction in 30 minutes.*
19. Aulton, M.E. and K.M.G. Taylor, *Aulton's Pharmaceutics: The Design and Manufacture of Medicines*. Fourth ed. 2013: Elsevier. p. 151-153.
20. Kuntsche, J., C. Decker, and A. Fahr, *Analysis of liposomes using asymmetrical flow field-flow fractionation: Separation conditions and drug/lipid recovery.* J. Sep. Sci. 35, 2012: p. 1993-2001.
21. *Wyatt Technology Corporation: The Eclipse ® AF4: The ultimate system for separating macromolecules, proteins, colloids, and nanoparticles.*
22. *Beckman Coulter Inc.: LS 13 320: Particle Size Analyzer.* p. 7-20.
23. Banga, A.K., *Transdermal and Intradermal Delivery of Therapeutic Agents: Application of Physical Technologies*. 2011: CRC press. p. 33-35.
24. *Diffusion Testing Fundamentals*. 28-04/2016; Available from: http://permegear.com/wp-content/uploads/2015/08/primer.pdf.
25. Yu, Y., et al., *Imaging-guided two-photon excitation-emission-matrix measurements of human skin tissues.* Journal of Biomedical Optics 17, 2012.

26. Claxton, N.S., T.J. Fellers, and M.W. Davidson. *Laser scanning confocal microscopy*. 03/05-2016; Available from: https://www.biomedicas.unam.mx/_administracion/_unidades_apoyo_inst/microscopia/lecturas/Intro_to_Laser_Scanning_Confocal_Microscopy.pdf.
27. Wilhelm, S., et al. *Confocal Laser Scanning Microscopy: Principles*. 03/05-2016; Available from: http://zeiss-campus.magnet.fsu.edu/referencelibrary/pdfs/ZeissConfocalPrinciples.pdf.
28. Belsey, N.A., et al., *Evaluation of drug delivery to intact and porated skin by coherent Raman scattering and fluorescence microscopies.* Journal of Controlled Release 174, 2014: p. 37-42.
29. *An Introduction to CARS Microscopy*. 20/04-2016; Available from: http://www.leica-microsystems.com/science-lab/an-introduction-to-cars-microscopy/.
30. Evans, C.L. and X.S. Xie, *Coherent Anti-Stokes Raman Scattering Microscopy: Chemical Imaging for Biology and Medicine.* Annual Reviews of Analytical Chemistry, 2008: p. 883-909.
31. Xie, X.S., J. Yu, and W.Y. Yang, *Living Cells as Test Tubes.* Sciencemag Volume 312, 2006: p. 228-230.
32. Petersen, S., A. Fahr, and H. Bunjes, *Flow Cytometry as a New Approach To Investigate Drug Transfer between Lipid Particles.* Molecular Pharmaceutics, Volume 7, Number 2, 2010: p. 350-363.
33. Verma, D.D., et al., *Particle size of liposomes influences dermal delivery of substances into skin.* International Journal of Pharmaceutics 258, 2003: p. 141-151.
34. *Lipophilic Tracers - DiI, DiO, DiD, DiA and DiR*. 09/05-2016; Available from: https://tools.thermofisher.com/content/sfs/manuals/mp00282.pdf.
35. *DiI Stain (1,1'-Dioctadecyl-3,3,3',3'-Tetramethylindocarbocyanine Perchlorate ('DiI'; DiIC18(3)))*. 09/05-2016; Available from: https://www.thermofisher.com/order/catalog/product/D282.
36. Parker, I. and M.D. Cahalan, *Handbook of Biomedical Nonlinear Optical Microscopy*. 2008: Oxford University Press. 759-762.
37. *OECD guideline for the testing of chemicals*. 10/05-2016; Available from: http://www.oecd-ilibrary.org/docserver/download/9742801e.pdf?expires=1462902029&id=id&accname=guest&checksum=ED4418F6FA9DA2CE51EF986E96303D22.
38. Badran, M.M., J. Kuntsche, and A. Fahr, *Skin penetration enhancement by a microneedle device (Dermaroller ®) in vitro: Dependency on needle size and applied formulation.* European Journal of Pharmaceutical Sciences 36, 2009: p. 511-523.
39. Spahic, E.T., *Evaluation of penetration enhancing effect of lipid-based formulations.* Master Thesis, University of Southern Denmark, 2015.

Appendix

Appendix I

Composition of the formulations:

Theoretical values for the composition of the 1.0 L TRIS buffer:

Mass of 10 mM TRIZMA pre-set crystals pH 7.4 is calculated:

$n = V \cdot c = 1\ L \cdot 0.01\ \frac{mol}{L} = 0.01\ mol$

$m = n \cdot M = 0.01\ mol \cdot 151.6\ \frac{g}{mol} = 1.516\ g$

Mass for 2.25% glycerol is calculated:

$m = 2.25\ g \cdot \frac{1L}{0.1L} = 22.5\ g$

Mass for 0.02% sodium azide is calculated:

$m = 0.02\ g \cdot \frac{1L}{0.1L} = 0.20\ g$

Appendix II

Table A1: The average values for the diameter (nm) of the particles, the average of the polydispersity indices and the standard deviation from the experiments by DLS (calculated from the raw data). The values are given as the average ± standard deviation.

Formulation	Diameter day 3 (nm)	PD index day 3	Diameter day 10 (nm)	PD index day 10	Diameter day 36 (nm)	PD index day 36	Diameter day 56 (nm)	PD index day 56
GMO_D0_15min_2	-	-	139.7 ± 1.7	0.199 ± 0.02	124.5 ± 1.1	0.131 ± 0.025	127.4 ± 2.2	0.113 ± 0.029
GMO_D0_30min_2	152.6 ± 2.8	0.133 ± 0.036	117.4 ± 2.2	0.181 ± 0.035	125.9 ± 1.2	0.173 ± 0.023	118.9 ± 1.3	0.159 ± 0.023
GMO_D0_30min_4	159.7 ± 3.0	0.139 ± 0.070	124.7 ± 1.8	0.193 ± 0.026	126.5 ± 2.4	0.161 ± 0.021	118.2 ± 1.8	0.155 ± 0.026
GMO_D0_60min_4	136.2 ± 2.7	0.157 ± 0.026	112.9 ± 1.9	0.206 ± 0.026	115.8 ± 1.8	0.189 ± 0.017	119.9 ± 1.6	0.185 ± 0.022
GMO_D0_30min_6	158.8 ± 3.5	0.166 ± 0.054	120.1 ± 2.5	0.199 ± 0.02	124.8 ± 1.0	0.173 ± 0.024	120.6 ± 1.5	0.172 ± 0.022
GMO_D0_60min_6	134.2 ± 3.3	0.158 ± 0.03	113.4 ± 1.4	0.217 ± 0.009	116.5 ± 2.1	0.180 ± 0.019	118.1 ± 2.3	0.194 ± 0.019
dGMO_D0_30min_8	-	-	143.7 ± 3.6	0.225 ± 0.014	171.0 ± 4.4	0.188 ± 0.072	153.8 ± 5.5	0.159 ± 0.037
dGMO_D0_60min_8	-	-	118.9 ± 2.2	0.188 ± 0.018	146.7 ± 2.0	0.185 ± 0.057	141.0 ± 3.7	0.161 ± 0.029
GMO_D1_15min_3	165.2 ± 3.8	0.177 ± 0.026	152.9 ± 3.5	0.217 ± 0.017	174.2 ± 3.8	0.188 ± 0.043	176.2 ± 3.1	0.155 ± 0.038
GMO_D1_30min_3	194.9 ± 3.8	0.13 ± 0.032	172 ± 3.4	0.172 ± 0.023	177.8 ± 2.9	0.135 ± 0.050	-	-
GMO_D1_15min_5	160.7 ± 3.3	0.18 ± 0.029	145.1 ± 2.5	0.203 ± 0.022	169.0 ± 4.5	0.131 ± 0.032	167.6 ± 3.8	0.131 ± 0.015
GMO_D1_30min_5	190.9 ± 3.6	0.147 ± 0.038	168.3 ± 4.9	0.169 ± 0.034	189.8 ± 4.2	0.127 ± 0.045	-	-
GMO_D3_15min_1	140.7 ± 2.5	0.113 ± 0.034	127.3 ± 2.4	0.137 ± 0.022	139.9 ± 2.2	0.121 ± 0.043	141.3 ± 2.5	0.098 ± 0.030
GMO_D3_30min_1	133.8 ± 2.6	0.123 ± 0.04	121.7 ± 1.3	0.155 ± 0.029	133.8 ± 3.8	0.170 ± 0.032	135.9 ± 3.6	0.151 ± 2.8
dGMO_D3_15min_7	-	-	127.4 ± 2.1	0.119 ± 0.028	139.9 ± 1.8	0.102 ± 0.026	143.9 ± 1.0	0.100 ± 0.024
dGMO_D3_30min_7	-	-	119.8 ± 1.7	0.132 ± 0.027	135.1 ± 2.1	0.124 ± 0.024	136.0 ± 2.9	0.129 ± 0.011

Table A2: The average values for the diameter (nm) of the particles, the average of the polydispersity indices and the standard deviation from the experiments after shaking by DLS (calculated from the raw data). The values are given as the average ± standard deviation.

Formulation	Diameter day 36 (nm)	PD index day 36	Diameter day 56 (nm)	PD index day 56
GMO_D0_15min_2	-	-	-	-
GMO_D0_30min_2	128.2 ± 1.9	0.180 ± 0.016	125.5 ± 2.3	0.186 ± 0.022
GMO_D0_30min_4	-	-	-	-
GMO_D0_60min_4	129.9 ± 2.0	0.220 ± 0.011	134.3 ± 1.9	0.232 ± 0.011
GMO_D0_30min_6	-	-	-	-
GMO_D0_60min_6	125.9 ± 1.4	0.205 ± 0.016	126.2 ± 1.7	0.224 ± 0.010
dGMO_D0_30min_8	-	-	-	
dGMO_D0_60min_8	160.9 ± 2.7	0.167 ± 0.066	181.4 ± 6.9	0.115 ± 0.077
GMO_D1_15min_3	-	-	-	-
GMO_D1_30min_3	-	-	-	-
GMO_D1_15min_5	-	-	-	-
GMO_D1_30min_5	-	-	-	-
GMO_D3_15min_1	-	-	-	-
GMO_D3_30min_1	135.4 ± 2.1	0.137 ± 0.033	141.0 ± 2.8	0.185 ± 0.024
dGMO_D3_15min_7	-	-	-	-
dGMO_D3_30min_7	136.7 ± 2.6	0.121 ± 0.026	142.6 ± 2.9	0.145 ± 0.025

Figure A1: Particle sizes for all nanoparticles by DLS after shaking.

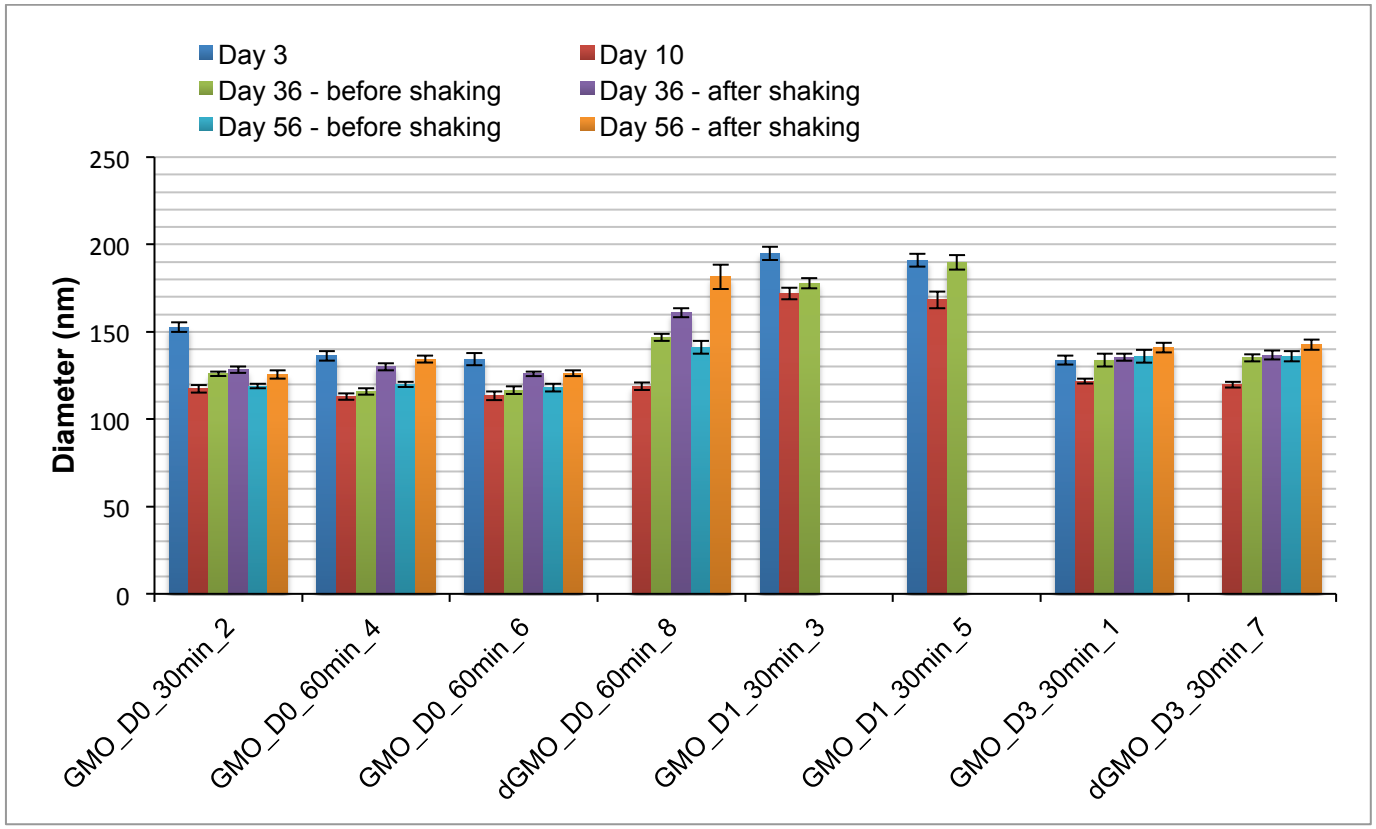

Table A3: Results for the diameter (nm) of the particles and the polydispersity indices from the experiments by DLS.

		Day 3				Day 10		Day 36				Day 56			
		First measurement		Second measurement		Third measurement		Fourth measurement		Fifth measurement (after shaking)		Sixth measurement		Seventh measurement (after shaking)	
Formulation	V_{sample} (µl)	Diameter (nm)	PD index	Diameter (nm)	PD index	Diameter (nm)	PD index	Diameter (nm)	PD index	Diameter (nm)	PD index	Diameter (nm)	PD index	Diameter (nm)	PD index
GMO_D3_ 15min_1	5	147.0	0.113	141.1	0.077	123.7*	0.096	135.8*	0.205			147.1*	0.074		
	5	144.5	0.137	142.9	0.082	123.2	0.127	140.7	0.167			144.5	0.117		
	5	141.4	0.146	140.1	0.135	124.7	0.155	140	0.115			139.9	0.129		
	5	144.8	0.069	141.4	0.068	125.7	0.116	140.3	0.116			143.4	0.113		
	5	143.4	0.061	143.5	0.116	127.9	0.131	142.1	0.086			145.4	0.114		
	5	140.7	0.109	138.7	0.132	127.7	0.126	143.4	0.013			141.2	0.118		
	10	139.3	0.164	139.5	0.079	132.2*	0.049	142.6	0.11			139.5	0.084		
	10	140.4	0.130	139.3	0.095	130.4	0.158	137.2	0.139			142.8	0.022		
	10	137.7	0.197	139.1	0.118	127.5	0.131	137.5	0.143			140	0.081		
	10	138.8	0.106	140.5	0.076	126.9	0.184	139	0.147			138.9	0.083		
	10	139.7	0.114	137.3	0.093	127.7	0.125	137.6	0.159			141.5	0.115		
	10	139.0	0.138	137.3	0.157	131.3	0.115	138.5	0.136			137.5	0.106		
GMO_D3_ 30min_1	5	139.3	0.101	134.9	0.135	119.5*	0.089	137.3*	0.172	140.0*	0.151	139.3*	0.125	145.2*	0.109
	5	134.6	0.154	134.8*	0.167	120.6	0.176	137.7	0.187	138.6	0.16	141.7	0.138	142.8	0.182
	5	136.7	0.128	134.7	0.057	121.9	0.160	139.5	0.221	134.9	0.115	138.8*	0.267	144.8	0.169
	5	138.9	0.131	134.9	0.127	123.4	0.137	136.8	0.183	135.1	0.121	138.3	0.097	145.8	0.219
	5	137.6	0.002	133.8	0.181	121.4	0.141	136.1	0.169	136.9	0.108	138.4	0.187	138.9	0.168
	5	134.6	0.129	134.5	0.112	120.6	0.214	134.3	0.176	136.1	0.09	137.5	0.158	142.6	0.143
	10	133.3	0.142	130.9	0.129	120.2	0.150	132.5	0.098	132.3*	0.196	139	0.125	141.3*	0.185
	10	132.7	0.157	132.4	0.150	121.6	0.151	135.7	0.143	136.6	0.181	134	0.201	138.8	0.172
	10	132.0	0.143	131.9	0.168	121.6	0.169	132.8	0.147	133.6	0.128	131.5	0.167	138.6	0.219
	10	131.7	0.108	133.0	0.078	123.8	0.111	129.9	0.171	136.9	0.136	135.2	0.105	140.3	0.184
	10	132.4	0.091	127.7	0.166	120.5	0.181	127.7	0.19	133.6	0.197	130.8	0.181	138.7	0.198
	10	133.0	0.139	133.0	0.090	123.3	0.120	129.1	0.185	131.5	0.138	132.6	0.148	138.4	0.199

GMO_D0_ 15min_2	5	47.0*	0.201	44.3*	0.208	142.1	0.163	124.7	0.137			129.2	0.099		
	5	46.4*	0.200	45.1*	0.237	139.6	0.196	125.8	0.093			132.2	0.144		
	5	46.8*	0.220	44.4*	0.204	141.4	0.211	123.9	0.154			129.3	0.115		
	5	46.2*	0.197	44.9*	0.221	138.2	0.189	123.4	0.127			130.7*	0.106		
	5	46.3*	0.185	43.7*	0.203	142.6	0.183	124.4	0.112			128.1*	0.102		
	5	46.9*	0.220	44.9*	0.216	139.0	0.202	122.6	0.142			126.9	0.093		
	10	100.1*	0.571	82.3*	0.261	139.3	0.202	125.6*	0.182			126	0.173		
	10	98.6*	0.571	81.3*	0.238	137.2	0.179	126.2	0.096			125.9	0.095		
	10	94.1*	0.571	81.2*	0.237	139.7	0.233	123.7	0.176			126.7	0.128		
	10	90.3*	0.472	81.8*	0.245	138.5	0.227	124.3	0.121			126	0.084		
	10	87.4*	0.327	83.3*	0.238	141.5*	0.154	124.7	0.131			125.1	0.085		
	10	88.4*	0.553	74.8*	0.237	139.3	0.200	125.3	0.15			126.7	0.118		
GMO_D0_ 30min_2	5	161.0*	0.219	155.0	0.117	118.8*	0.176	126.8*	0.231	133.6*	0.194	118.4*	0.164	128.5	0.202
	5	152.6	0.204	153.4	0.126	113.5	0.146	126.8	0.197	129.8	0.188	118.4	0.146	129.3	0.177
	5	157.7*	0.201	154.3	0.103	115.5	0.136	127.8	0.173	126.5	0.158	118.2	0.13	128.6	0.193
	5	156.8	0.185	155.4	0.115	115.3	0.164	126.2	0.155	128.7	0.192	120.4	0.185	123.9	0.222
	5	156.6*	0.138	154.4	0.073	115.9	0.221	126.6	0.2	130.2	0.192	120.7	0.16	125.8	0.166
	5	156.3	0.154	158.0	0.157	119.1	0.125	126.2	0.159	131.7	0.175	119.9	0.143	125.8	0.208
	10	154.9*	0.157	149.8	0.130	116.4	0.200	123.1*	0.212	127.8*	0.173	124.7*	0.135	125.8	0.207
	10	150.4	0.177	151.8	0.110	117.8	0.219	124.5	0.207	127.2	0.188	118.9	0.185	124.4	0.176
	10	151.8	0.138	153.1	0.087	120.2	0.196	126.1	0.154	127	0.165	119.8	0.128	123.2	0.17
	10	151.8	0.106	147.6	0.135	118.4	0.172	125.7	0.187	127.9	0.168	116.6	0.173	122.4	0.193
	10	150.2	0.145	149.6	0.095	120.7	0.189	125.2	0.138	126	0.163	117.7	0.188	124.9	0.144
	10	149.8	0.190	149.6	0.117	118.3	0.226	123.8	0.159	126.6	0.206	118.8	0.151	123	0.173

GMO_D1_ 15min_3	5	172.6	0.145	168.1	0.186	156.6*	0.239	179.3	0.207			178.6	0.19		
	5	170.9	0.197	169.2	0.139	158.4*	0.238	176.8	0.203			179.7	0.148		
	5	166.6	0.202	165.9	0.179	150.3	0.237	179.6	0.141			180.3	0.082		
	5	170.9	0.195	166.3	0.200	159.0	0.228	177.6	0.158			178.5	0.171		
	5	168.3	0.173	162.1	0.195	149.0	0.231	173.3	0.188			174.9	0.146		
	5	166.8	0.205	168.2	0.134	155.3	0.211	176.1	0.158			177.4	0.167		
	10	165.8	0.208	160.3	0.190	151.6*	0.137	166.2*	0.199			175.2*	0.191		
	10	166.1	0.166	164.4	0.127	150.2	0.225	171.2	0.173			177.1	0.229		
	10	159.4	0.218	160.3	0.167	150.9	0.198	172.1	0.232			172.4	0.142		
	10	162.3	0.180	164.1	0.128	155.0	0.220	169.3	0.211			174.1	0.172		
	10	162.2	0.159	162.2	0.190	150.1	0.184	171.8	0.127			174	0.145		
	10	163.4	0.190	159.4	0.179	156.1	0.217	169.6	0.274			171.1	0.116		
GMO_D1_ 30min_3	5	194.5	0.144	191.3	0.156	167.9*	0.150	182	0.108						
	5	199.2	0.176	193.3	0.120	171.8	0.170	180.9	0.07						
	5	197.6	0.126	192.6	0.135	166.1	0.159	179.5	0.138						
	5	194.3	0.117	191.5	0.158	173.4	0.195	177.3	0.114						
	5	190.6	0.121	190.2	0.123	168.2	0.144	175.4	0.07						
	5	198.0	0.158	189.4	0.174	167.4	0.150	177.9	0.082						
	10	206.6*	0.000	192.9	0.112	175.6*	0.192	193.4*	0.093						
	10	201.3	0.041	195.0	0.165	174.8	0.196	181.4	0.191						
	10	201.8	0.096	195.6	0.127	173.2	0.140	177.9	0.15						
	10	199.7	0.080	197.2	0.167	175.1	0.174	174.1	0.172						
	10	198.9	0.132	193.6	0.115	174.9	0.200	173.9	0.184						
	10	195.9	0.101	189.2	0.144	174.7	0.193	175.3	0.209						

GMO_D0_ 30min_4	5	173.4*	0.227	158.6	0.207	122.2	0.199	125.0*	0.166			120.6*	0.101		
	5	161.7*	0.222	157.2	0.212	126.7	0.180	125.9	0.16			114.6*	0.15		
	5	158.3	0.187	162.5	0.194	122.4	0.234	127.8	0.175			121.6*	0.165		
	5	156.2	0.223	159.5	0.175	124.2	0.213	128.9	0.136			116	0.188		
	5	157.5	0.214	153.4	0.216	125.1	0.180	130.1	0.132			117	0.114		
	5	156.2	0.163	163.1	0.198	124.5	0.204	128.2	0.165			118.3	0.169		
	10	158.3	0.150	160.5	0.090	123.4*	0.185	128.8*	0.154			117.4	0.178		
	10	158.5	0.132	156.2	0.063	124.0	0.204	123.4	0.159			121.5	0.141		
	10	158.5	0.134	160.9	0.003	125.2*	0.438	127.2	0.154			117.1	0.173		
	10	161.2	0.152	163.3	0.055	125.1	0.181	125.5	0.178			120	0.118		
	10	165.3	0.131	163.2	0.038	128.3	0.135	125.2	0.147			117	0.158		
	10	162.7	0.122	162.0	0.003	124.1	0.199	122.5	0.203			119.2	0.152		
GMO_D0_ 60min_4	5	140.2	0.156	139.0	0.181	111.5*	0.231	116.0*	0.17	131.0*	0.223	120.9*	0.204	134.7*	0.237
	5	139.0	0.166	136.0	0.165	111.0	0.172	118.6	0.192	128.9	0.232	122.1	0.183	136.3	0.238
	5	136.8	0.191	136.3	0.192	112.7	0.211	115.4	0.188	128.5	0.229	121.4	0.195	134	0.23
	5	141.2	0.169	140.5	0.184	110.8	0.235	113.8	0.202	132.3	0.226	122.3	0.178	134.5	0.235
	5	137.6	0.164	137.2	0.189	110.4	0.235	115.6	0.201	132	0.212	120.1	0.212	134.1	0.239
	5	140.3	0.143	133.3	0.134	113.6	0.215	115.7	0.157	130.9	0.215	119.9	0.164	137.3	0.199
	10	132.5	0.159	135.9	0.111	112.5*	0.237	116.0*	0.214	133.0*	0.237	119.7	0.149	134.2	0.236
	10	136.6	0.110	133.8	0.152	115.7	0.214	117.1	0.201	132.8	0.201	119.5	0.201	136.8	0.238
	10	133.5	0.149	132.2	0.169	113.6	0.199	115.3	0.207	130	0.233	118	0.182	131.6	0.237
	10	134.1	0.172	133.2	0.147	111.9	0.195	118.4	0.165	128.4	0.232	119.5	0.204	133	0.234
	10	135.6	0.124	135.4	0.174	114.9	0.156	112.8	0.183	127.7	0.211	118.6	0.213	133.9	0.235
	10	133.6	0.172	134.7	0.101	114.8	0.225	114.8	0.194	127.6	0.211	117.5	0.159	131.8	0.231

GMO_D1_ 15min_5	5	163.9	0.212	158.1	0.207	139.5*	0.226	170.8*	0.185			173.0*	0.216		
	5	166.6	0.188	160.8	0.223	141.4	0.228	167.6	0.184			170.8*	0.158		
	5	162.3	0.191	164.2	0.167	141.4	0.186	175.1	0.087			171.2	0.122		
	5	164.7	0.149	164.1	0.195	143.2	0.201	170.2	0.124			172.2	0.14		
	5	165.6	0.172	164.8	0.189	145.0	0.221	162.6	0.158			169.2	0.124		
	5	160.4	0.223	161.3	0.200	146.4	0.212	170.6	0.113			173.3	0.12		
	10	158.9	0.193	161.1	0.178	146.2	0.158	171.4*	0.213			168.1	0.133		
	10	156.7	0.200	157.1	0.189	143.5	0.192	173.5	0.107			164.8	0.11		
	10	157.7	0.176	160.1	0.131	149.3	0.180	168.2	0.122			163.1	0.158		
	10	156.4	0.196	159.3	0.128	146.3	0.220	167.7	0.161			166.3	0.144		
	10	155.1	0.187	158.4	0.156	147.3	0.212	172.8	0.095			163.6	0.117		
	10	157.9	0.165	162.4	0.113	146.3	0.220	161.3	0.158			163.8	0.143		
GMO_D1_ 30min_5	5	194.4	0.160	185.8	0.129	163.2	0.154	196.9	0.101						
	5	193.4	0.177	186.9	0.132	165.8	0.145	194.7	0.088						
	5	198.4	0.074	191.7	0.168	164.1	0.105	191.1	0.144						
	5	191.1	0.127	190.2	0.131	162.6	0.182	194.1	0.099						
	5	194.6	0.060	189.7	0.096	165.4	0.193	189.2	0.132						
	5	191.3	0.122	185.4	0.165	164.1	0.171	191.9	0.041						
	10	192.4	0.221	182.0	0.168	173.9*	0.196	186.2	0.188						
	10	196.1	0.168	188.9	0.130	174.2	0.221	186.4*	0.156						
	10	194.5*	0.144	190.4	0.203	173.4	0.209	187.7	0.127						
	10	192.3	0.169	192.3	0.139	173.6	0.171	184.1	0.174						
	10	191.3	0.148	189.2	0.194	174.2	0.179	185.8	0.184						
	10	192.1	0.157	191.4	0.133	170.5	0.127	186.3	0.122						

GMO_D0_ 30min_6	5	166.0	0.229	162.3	0.211	117.9*	0.222	126.5	0.169			118.6*	0.212		
	5	161.7	0.216	157.7	0.231	118.6	0.197	125.5	0.199			122	0.169		
	5	159.5	0.199	157.7	0.211	117.7	0.191	125.2	0.177			121.4	0.155		
	5	161.1	0.198	162.9	0.210	115.6	0.230	125.1	0.165			122.1	0.199		
	5	163.4	0.187	159.9	0.227	119.2	0.189	125.6	0.122			122.2	0.166		
	5	159.1	0.219	163.9	0.184	119.3	0.205	124.9	0.173			117.6	0.181		
	10	157.2	0.152	157.5	0.133	121.9	0.196	127.0*	0.199			121.6*	0.225		
	10	157.3	0.147	151.9	0.149	120.7	0.219	124.9	0.216			121.4	0.141		
	10	152.7	0.136	156.9	0.037	121.9	0.189	124.5	0.187			120.1	0.145		
	10	158.6	0.082	153.9	0.103	119.4	0.226	123	0.166			120.1	0.204		
	10	156.3	0.149	157.0	0.087	122.9	0.162	123.8	0.163			120.7	0.173		
	10	157.2	0.125	158.5*	0.046	124.3	0.182	123.7	0.161			118.7	0.191		
GMO_D0_ 60min_6	5	140.0	0.189	133.2	0.197	109.7*	0.237	111.8*	0.193	131.2*	0.239	119.0*	0.181	129.9	0.217
	5	139.0	0.157	135.5	0.189	111.6	0.221	118.5	0.212	126.1	0.213	121.1	0.204	126.3	0.21
	5	138.7	0.171	137.6	0.106	113.2	0.215	115.2	0.183	127.4	0.209	121.5	0.192	126.7	0.228
	5	139.5	0.191	135.9	0.135	113.5	0.218	117.4	0.175	127.7	0.178	118.7	0.193	126.7	0.218
	5	134.3	0.146	133.1	0.162	114.9	0.230	113.4	0.189	126.1	0.214	118.7	0.215	125.9	0.226
	5	139.9	0.143	134.2	0.181	113.2*	0.238	115	0.188	126.4	0.22	119	0.203	126.6	0.205
	10	128.1	0.155	133.0	0.122	115.0	0.202	115.3*	0.146	123.1*	0.225	116.8	0.217	127.1*	0.198
	10	133.8	0.173	131.7	0.064	114.3	0.211	114.3	0.201	127.3	0.226	120.1	0.154	127.2	0.235
	10	131.6	0.154	130.3	0.181	112.0	0.228	119.6	0.159	124.7	0.195	115.7	0.204	126.2	0.233
	10	132.6	0.168	132.2	0.161	112.9	0.225	117.5	0.181	124.4	0.219	117.7	0.183	122.9	0.227
	10	131.6	0.164	132.1	0.140	111.7	0.207	115.4	0.152	123.6	0.191	114.7	0.196	124.9	0.226
	10	132.6	0.189	131.1	0.158	115.1	0.211	118.8	0.164	125.1	0.185	115.3	0.171	124.8	0.237

dGMO_D3_ 15min_7	5	126.6	0.145					141.2*	0.137			149.2*	0.063		
	5	126.3	0.105					141	0.111			143.7	0.106		
	5	124.5	0.115					139.4	0.136			144.8	0.083		
	5	128.2	0.125					141.9	0.072			145.4	0.047		
	5	123.6	0.160					141.3	0.08			143.5	0.085		
	5	128.3	0.085					136	0.099			144.1	0.124		
	10	127.7	0.111					140.4	0.16			150.1*	0.139		
	10	128.9	0.165					141.9	0.093			143.9	0.122		
	10	126.6	0.067					140.5	0.083			145.2	0.088		
	10	130.3	0.115					139	0.109			143.6	0.121		
	10	130.4	0.110					137.8	0.092			141.9	0.116		
	10	127.6	0.121					139.4	0.084			143.2	0.11		
dGMO_D3_ 30min_7	5	116.5	0.117					135.2	0.103	136.1*	0.145	134.8*	0.147	144.5	0.167
	5	118.2	0.154					139.4	0.122	139.3	0.123	139.8	0.123	144.8	0.141
	5	119.8	0.103					134.8	0.125	138.5	0.097	140.1	0.133	147.3	0.138
	5	118.5	0.128					136.6	0.176	140.5	0.104	137.2	0.121	144.4	0.118
	5	121.1	0.104					137.4	0.096	137.6	0.149	137.2	0.117	145	0.086
	5	118.9	0.104					135.4	0.106	138	0.098	138.6	0.125	142.1	0.153
	10	122.0*	0.122					136.1*	0	136.1*	0.091	133.7*	0.1	137.6*	0.185
	10	121.0	0.121					135.1	0.118	134.7	0.12	132.6	0.147	141	0.158
	10	119.2	0.152					134.2	0.138	132.2	0.175	134.3	0.114	142.4	0.175
	10	121.5	0.121					133.1	0.15	134.3	0.114	133.4	0.136	139.9	0.152
	10	122.1	0.158					132.7	0.131	135	0.135	133.8	0.145	138	0.156
	10	120.5	0.187					132.6	0.1	137.8	0.097	133.2	0.128	139.2	0.153

dGMO_D0_ 30min_8	5	138.6*	0.220					166.0*	0.236			158.8	0.188		
	5	137.8	0.239					175.1	0.222			159.7	0.122		
	5	143.2	0.237					171	0.222			163.4	0.08		
	5	140.1	0.239					166.2	0.225			156.7	0.187		
	5	142.7	0.225					167.7	0.237			156.6	0.16		
	5	138.8	0.231					166.8	0.238			151.9	0.217		
	10	144.8	0.236					181.0*	0.053			149.2*	0.181		
	10	145.5	0.225					178	0.054			147.3	0.133		
	10	144.9	0.217					179.3*	0			149.7	0.156		
	10	147.4	0.195					176.3*	0			151.3	0.166		
	10	146.8	0.231					175.9*	0			147.7	0.17		
	10	149.1	0.205					172.1	0.12			148.9	0.174		
dGMO_D0_ 60min_8	5	119.3*	0.145					153.4*	0.144	169.0*	0.165	143.3*	0.134	184.9	0.101
	5	115.9	0.202					147.2	0.237	166.9	0.191	144.4	0.126	185.4	0.094
	5	117.5	0.171					143	0.239	162.2	0.203	143.6	0.175	187.6	0.14
	5	119.7	0.165					145.1	0.238	159.6	0.239	142.6	0.194	188.8	0.148
	5	116.4	0.190					148.8	0.238	163.5	0.251	146.6	0.194	185.9	0.213
	5	116.8	0.208					149.5	0.232	159.9	0.238	143.2	0.173	182.5	0.238
	10	117.2	0.219					149.1*	0.162	162.4	0.194	137.5	0.143	174.8	0.043
	10	119.9	0.160					145.5	0.13	160	0.156	143.8	0.165	174.0*	0
	10	121.0	0.195					148.9	0.164	161	0.086	136.2	0.117	169.6*	0
	10	120.2	0.188					147.3	0.12	158.2	0.098	138.6	0.16	167.5*	0
	10	121.6	0.182					146	0.105	158.1	0.081	136.5	0.199	171.6	0.017
	10	121.5	0.185					145.7	0.145	158.1	0.102	138.1	0.128	171.3	0.038

*Unreliable measurements due to a PD index too high, PD index at zero or a correlation function not being stable.

Table A4: Average particle sizes and PD indices ± standard deviation of the formulations containing ethanol (from the DiI stock solution).

Formulation	Diameter (nm)	PD index	Diameter after shaking	PD index after shaking
dGMO_D0_60min_8	142.1 ± 6.8	0.159 ± 0.065	132.5 ± 2.6	0.198 ± 0.036
dGMO_D3_30min_7	141.5 ± 2.6	0.079 ± 0.036	141.2 ± 4.0	0.087 ± 0.044

Figure A2: Measurements of formulations containing ethanol compared to the measurements made on day 56.